Declaration

I declare that this dissertation is my unaided work. It is being submitted for the degree of Master of Science in Engineering degree at the University of the Witwatersrand, Johannesburg. It has not been submitted before for any degree or examination to any other University.

.....Rodwell Muzavazi.....

(Signature of Candidate)

……14……. day of ……June…… year ……2022…….

Dedication

I dedicate this dissertation to God, my family, friends, and future family.

Acknowledgements

I would like to extend my sincere gratitude to my supervisor and advisor, Prof. Olutayo O. Oyerinde, for going above and beyond to help me from the beginning of this research to its completion. If it were not for him, I would not have been able to reach this far in this journey.

I would also want to thank my family for their unwavering support, encouragement, love, and prayers.

For financial support, I would like to thank the CeTAS program and the South Africa NRF Competitive Program (funding) for Rated Researchers with grant number 118547 through Prof. Olutayo O. Oyerinde.

Finally, l would like to express my utmost appreciation to God for guiding me throughout this journey. I doubted myself many times, but God always spoke to me through the people around me and my advisor, which kept me going.

Table of Contents

List of Figures

List of Tables

Abbreviations

5G	Fifth-Generation
OTFS	Orthogonal Time Frequency Space
ICI	Inter-Carrier Interference
OFDM	Orthogonal Frequency Division Multiplexing
MIMO	Multiple Input Multiple Output
CSI	Channel State Information
UE	User Equipment
BS	Base Station
IUI	Inter-User Interference
3GPP	Third Generation Partnership Project
LTE	Long Term Evolution
4G	Fourth-Generation
DD	Delay-Doppler
TF	Time-Frequency
ML	Maximum Likelihood
ISFFT	Inverse Symplectic Finite Fourier Transform
CP	Cyclic Prefix
QAM	Quadrature Amplitude Modulation
DFT	Discrete Fourier Transform
OoB	Out Of Band

ISI	Inter-Symbol Interference
AWGN	Additive White Gaussian Noise
SFFT	Symplectic Finite Fourier Transform
3D-SOMP	Three Dimensional-Structured Orthogonal Matching Pursuit
EM-VB	Expectation Maximization-based Variational Bayesian
DDSP	Delay-Doppler Subspace Pursuit
CE	Channel Estimation
NMSE	Normalized Mean Square Error
MMSE	Minimum Mean Square Error
ZF	Zero Forcing
NSE	Neumann Series Expansion
GS	Gauss-Seidel
CS	Compressive Sensing
BER	Bit-Error-Rate
SNR	Signal-Noise-Ratio
QoS	Quality of Service
CIR	Channel Impulse Response
LS	Least Square
PDF	Probability Density Function
BE	Bandwidth Efficiency
SOS	Second Order Statistics
LTI	Linear Time Invariant

BP	Basis Pursuit
BPDN	Basis Pursuit De-Noising
PAPR	Peak-to-Average Power Ratio
FDD	Frequency Division Duplex
ULA	Uniform Linear Array
NPI	Noise Plus Interference
CoSaMP	Compressive Sampling Matching Pursuit

Chapter 1 – Introduction

1.1 Overview

Fifth-generation (5G) and future generation systems are expected to provide efficiency in data transmission and network connectivity under high-Doppler scenarios like vehicle-to-vehicle, vehicle-to-infrastructure, high-speed trains, and mm-Wave [1-3]. The Orthogonal Time Frequency Space (OTFS) scheme introduced in [4] addresses inter-carrier interference (ICI) in high-Doppler scenarios to produce a reliable system with a low-complexity receiver design and good performance advantage over Orthogonal Frequency Division Multiplexing (OFDM) [5-9]. The combination of OTFS and massive multiple-input multiple-output (MIMO) addresses the implementation and complexity of massive MIMO in 5G and future generation systems [10]. The OTFS massive MIMO system exhibits reliable connection and high data throughput in high-Doppler scenarios, demonstrating high Doppler shift compensation. Good channel state information (CSI) and efficient data detection allow the system to enjoy the benefits of the combination of OTFS and massive MIMO. As a result, this motivates our current research work to develop a more efficient channel estimation scheme and data detection technique that minimizes errors and with lower complexity that allows for it to be used in less powerful/low-cost hardware.

This chapter provides a summary of the background of the technologies considered in this research work. Following will be the research question and contributions of this research. Finally, the organization of the remaining chapters is outlined.

1.2 Massive MIMO

The exponential increase of smartphones, computers and applications on devices requiring higher data throughput to function properly surpasses the capacity increase of wireless communication networks, which focuses on 5G networks and future networks. Users will expect highly reliable communication. Researchers have been exploring MIMO systems technology in wireless and wired communication systems for several years now [11]. While standard and current techniques are challenging to provide ultra-fast speeds and reliable connectivity, theoretical and practical experiments show great potential and evidence that massive MIMO improves network speeds vastly [12]. 5G and future generation systems aim at providing higher spectrum efficiency and increase in data throughput.

Massive MIMO yields the advantages of MIMO technology at a massive scale in wireless communication systems. Massive MIMO utilizes huge number of antennas both in the

transmission and receiver to exploit multi propagation in wireless systems. Massive MIMO serves many users with high gain and improves spectrum efficiency, energy efficiency, and reliability. Moreover, in massive MIMO channels, the receiving antennas receive the transmitted signal with a statistically similar gain because of the space diversity introduced by the system's massive number of antenna elements [4].

A diversity technique was applied in [13] To minimize fading effects and increase the system's strength to fight interference. The transmission antennas *M* and receiver *N* in Figure 1.1 take advantage of wireless channel diversity, resulting in reliable connectivity. In the massive MIMO systems, the enormous magnitude of antennas is directly proportional to the amount of data released to serve more user equipment (UE). Massive MIMO has more base station (BS) antenna elements than UEs per cell to reduce interference.

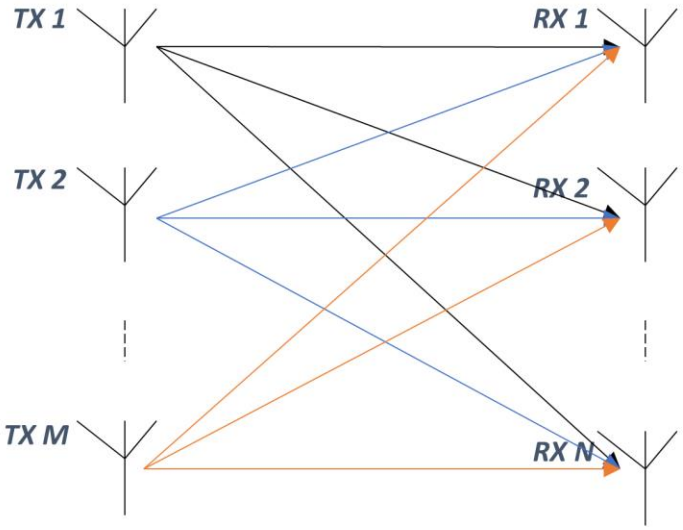

Figure 1.1: Generic Massive MIMO system with M transmitters and N receivers [11]

The availability of many antennas makes it more feasible to process and or combine the multi-antenna signals jointly and thus improve the systems' integrity [11]. The massive number of antennas in massive MIMO will boost the link reliability through spatial diversity, boost the degrees-of-freedom in the spatial domain, and help improve the overall performance of the communication system. BSs can avoid propagation into unwanted directions to eliminate harmful interference to the signal, leading to low latency [12]. Massive MIMO splits the

transmit power amongst huge propagation paths to transmit signals, increasing the capacity without consuming extra radiofrequency and, as a result, increasing spectral efficiency. A massive MIMO system reduces the transmission power and alleviates intracell interference [14]. Massive MIMO aims at producing high data throughput and better performance over time-selective channels, frequency-selective channels, and high-Doppler scenarios. The high data throughput in massive MIMO is separated at the receivers by algorithms that depend on channel estimation between all the transmitters and receivers. A massive MIMO system can exploit both transmitter and receiver diversity since the data is propagated through different paths, maintaining reliable communications [15]. Massive MIMO was initially introduced to improve bandwidth efficiency; mm-Wave spectral resources boost the system bandwidth. Multi-layer and ultra-dense networks are distributed to increase bandwidth use in a vast area [16]. This is shown by the massive MIMO network system's ability to reuse the radio frequency resources in different cells. Massive MIMO implements hundreds to thousands of antennas to simultaneously serve dozens of user equipment. Simultaneously serving tens of UEs brings about spectral efficiency in massive MIMO. More antennas result in more energy efficiency. It helps propagate energy with a very narrow beam in small regions where the UEs are located. As a result, it also alleviates inter-user interference (IUI) [16]. The degrees of freedom brought about by massive MIMO due to the enormous antenna elements can eliminate interference.

1.3 Orthogonal Time Frequency Space

OFDM works well in Third Generation Partnership Project (3GPP), Long Term Evolution (LTE), and fourth-generation (4G) communication systems. OFDM was introduced to also deal with the time-dispersive nature of the mobile channels and should utilize as little bandwidth as possible and decrease interference amongst systems on adjacent channels. However, as efficient as OFDM has proven, it breaks down when the channel rapidly changes in high Doppler scenarios. OTFS modulation is a modulation scheme with great potential in communication systems. The unreliability of OFDM and other multi-propagation techniques in communication systems has motivated research in OTFS for 5G and future networks. OTFS seems to exhibit better performance in high mobility scenarios like vehicle-to-vehicle, vehicle-to-infrastructure, high-speed trains, and mm-Wave. A high-speed train traveling at 350kmph and above can experience a maximum Doppler shift of about 650 Hz, induced for a carrier frequency of 2 GHz. The coherence time of the channel is approximately the inverse of its maximum Doppler shift; the channel state information changes very fast, which precise channel estimation is essential and requires high pilot overhead in an OFDM system [1]. OFDM is

known to have great capacity in frequency-selective channels. The ability remains consistent as long as conditions like Gaussian modulation alphabet, channel state information, long codewords, and unlimited receiver complexity are assumed. The assumptions prove to be inconsistent in OFDM. The input visualizes a 2D convolutional channel in the delay-Doppler (DD) domain and a multiplicative channel in the time-frequency (TF) domain. OTFS can be applied as a pre-and post-processing block to filtered OFDM systems, thus allowing architectural compatibility with LTE. OFDM may experience significant inter-carrier interference in high mobility scenarios because of the more extensive Doppler spread of time-varying channels [17]. The measurement of OTFS is done in a longer observation time, making channel estimation easier. In OTFS, the fading, time-varying wireless channel is converted to a time-independent channel with a constant complex channel gain for all symbols. All symbols are subjected to almost the same channel gain when transmitted by the OTFS system, which lowers the pilot overhead ratio and the complexity associated with physical adaptation [18]. OTFS can be brought down to an OFDM if the two-dimension (2D) basis functions are sub-channel carriers or can be visualized as a single-carrier transmission generalization. The basis pulses' localization is not only in the delay domain but also in the Doppler domain [1].

Due to the spread-spectrum nature of OTFS, the pilot power is evenly spread in time over the time-domain (TD) plane. As a result, the even channel gain by all the symbols in the OTFS transmission frame dramatically reduces the channel estimation pilot overhead in a fast-varying channel. An almost time-invariant channel in DD leads to asymmetric and straightforward coupling between the channel and modulation symbols [19]. As a result, this increases the pilot symbol power over data symbol power without affecting the peak transmitted power [5]. There can be linear receivers and non-linear receivers. Non-linear receivers trade-off good performance with high complexity cost. However, a linear receiver is simpler but performs more poorly than a non-linear receiver [20]. The DD representation of the channel impulse response requires fewer parameters for estimation because it yields a sparse channel representation [3]. Full diversity can be obtained through an approximately designed equalizer in the TF domain. The sparsity nature and lower variability nature of the channel due to lower variability in the DD make OTFS far more implementable and robust [18]. As a result, a diminution of the standard deviation of power variations from 4 dB to 0.1 dB is achieved [21].

OTFS consists of 2D transformation at the transmitter and receiver, as shown in Figure 1.2. The transmitter first maps 2D Delay-Doppler information symbols $\boldsymbol{x}$ to symbols in time-frequency domain $\boldsymbol{X}$ via an *inverse* symplectic finite Fourier transform (ISFFT). The symbols

X in TF are mapped to the TF symbols ***S*** via the transmitting windowing function to complete the OTFS transform. The following step is the transformation of the symbols ***S*** in TF to time-domain symbols ***s*** in the time domain via the Heisenberg transform to transmit in the channel with the addition of cyclic prefix (CP) symbols. The Heisenberg transformation works similarly to the OFDM transformation, so the OTFS is sometimes described as the pre-processing and post-processing block of the OFDM.

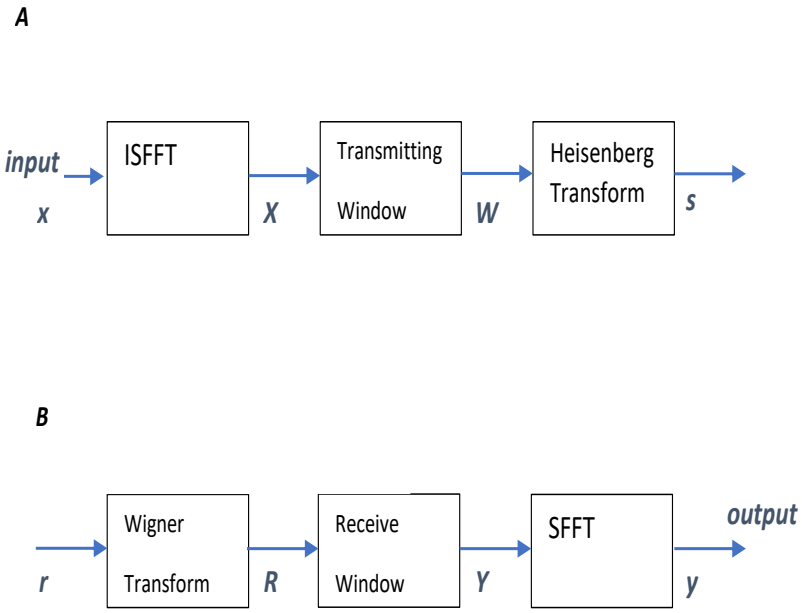

Figure 1.2: OTFS Model with windowing: (A) OTFS Modulator with Windowing, (B) OTFS Demodulation with Windowing

At the receiver, opposite operations are performed. The received signal ***r*** in the time domain is first mapped to the TF symbols ***R*** via the inverse Heisenberg transform. The Wigner transform performs OFDM demodulation and removal of the cyclic prefix. The TF symbols ***R*** are mapped to the TF symbols ***Y*** via the receiving windowing function. Lastly, the TF symbols ***Y*** are mapped to the 2D DD symbols ***y*** via a *symplectic* Fourier transform.

1.3.1 Modulation

OTFS is assumed to be a 2D transformation. The information symbols ***x***, in the DD domain at the transmitter, are mapped into the time-frequency domain through the finite Fourier Transform. The data sequence considered is the quadrature amplitude modulated (QAM) with *MN* length and is initially arranged into a 2D data block. The DD block in 2D maps the

2D block in TF, and this is obtained by utilizing an *inverse* symplectic Finite Fourier Transform as illustrated as [18].

$$\boldsymbol{X} = \boldsymbol{F}_M \boldsymbol{x} \boldsymbol{F}_N^H \quad . \tag{1.1}$$

Where $\boldsymbol{F}_M$ and $\boldsymbol{F}_N^H$ are complex $M \times M$ and $N \times N$ discrete Fourier transform (DFT) matrices, respectively. The TF domain symbol $\boldsymbol{X}$ passes through the windowing function to result in,

$$\boldsymbol{S} = \boldsymbol{X} \odot \boldsymbol{W}^{tx}. \tag{1.2}$$

Windowing matrix $\boldsymbol{W^{tx}}$ in (1.2) can be used to eliminate inter-cell interference by randomizing phases of the transmitted symbols.

$\boldsymbol{S}$ is fed into the Heisenberg Transform or OFDM, where it will transform into OTFS. To account for the inter-symbol interference between the blocks, the Heisenberg Transform usually adds a cyclic prefix for every OFDM symbol [4]. The windowing function, cyclic prefix and postfix technology effectively reduce out of band (OoB) power in OTFS [22]. Adding cyclic prefix symbols to the TF domain signal that has been produced after the windowing function will give,

$$\boldsymbol{S_{CP}} = \boldsymbol{A_{CP}} \boldsymbol{F_M^H} \boldsymbol{W}. \tag{1.3}$$

Where $\boldsymbol{A_{CP}}$ is the CP addition matrix, and $\boldsymbol{W}$ is the $M \times N$ matrix containing time-frequency samples $\boldsymbol{S}$. The $(M \times M_{CP}) \times N$ matrix $\boldsymbol{S_{CP}}$ includes the time domain OFDM transmit signals on its column. The OTFS signal at the baseband can be formed by using parallel to serial conversion of $\boldsymbol{S_{CP}}$ as $\boldsymbol{s}$ = *vec* { $\boldsymbol{S_{CP}}$ }.

It is also crucial to note that the bi-orthogonality property of the pulse shapes eliminates the inter-symbol interference (ISI) in OTFS [1]. A transmit pulse and associated receive pulse

whose inner products are bi-orthogonal with respect to translations by integer multiples of time T and frequency Δf.

1.3.2 Demodulation

The *k-th* element of the received samples **r**, which is $(M \times M_{CP}) \times N$ matrix with length L after the time-variant channel $h_{k,l}$ with length L is expressed as

$$r_{k,l} = \sum_{l=0}^{L} h_{k,l} s_{k-l} + v_k, \tag{1.4}$$

where v_k is the additive white Gaussian noise (AWGN) at the receiver. With the assumption that $M_{CP} \geq L$, the received OFDM symbols do not have inter-symbol interference. In (1.4), the received signal is a superposition of reflected copies of the transmitted signal, where each copy is delayed by path delay τ, frequency shifted by the Doppler shift v and weighted by the time-independent complex-valued delay-Doppler impulse response $h_{k,l}$ for that particular τ and v. After the Wigner transformation (inverse Heisenberg transformation),

$$\boldsymbol{R} = \boldsymbol{F_M R_{CP} R_n} + \bar{\boldsymbol{v}}_n, \tag{1.5}$$

where the inverse vectorization of $\boldsymbol{R}_n$ is performed as $\boldsymbol{R}_n$ = invec { **r** }. The complex 2D data block $\boldsymbol{y}$ is obtained by a receive windowing matrix $\boldsymbol{W^{rx}}$ first. Then, the *symplectic* finite Fourier transform (SFFT) is applied to realize $\boldsymbol{y}$ in the delay-Doppler domain.

$$\boldsymbol{Y} = \boldsymbol{R} \odot \boldsymbol{W^{rx}}, \tag{1.6}$$

$$\mathbf{y} = \boldsymbol{F_M^H Y F_M}. \tag{1.7}$$

The process in (1.7) can also be stipulated as:

$$\boldsymbol{y}_{k,l} = \sum_{m=0}^{M-1} \sum_{n=0}^{N-1} \boldsymbol{x}_{\boldsymbol{m,n}} \boldsymbol{H}_{k-m,l-n} b_{k,l}\,(m,n) + v_{k,l}\,, \qquad (1.8)$$

where k=0, ……., M-1, and l = 0, ..., N-1, $v_{k,l}$ is the additive Gaussian noise and

$b_{k,l}(m,n) = e^{\frac{-J2\pi k(l-n)}{N(M+N_{CP})}}$. In [18], it is evident that the OTFS output samples at the receiver, $y_{k,l}$ can be achieved as the 2D circular convolution of the QAM data symbols $x_{k,l}$, where all the symbols experience a uniform time-invariant channel impulse $\boldsymbol{H}_{k-m,l-n}$ response in the delay-Doppler domain. Moreover, with the support of the windowing function increasing along the time and frequency domain, this leads to the narrowing of the filtering function in (1.8) which is the periodic function with periods ($M\Delta\tau, N\Delta v$) in delay and Doppler respectively. As a result, OTFS has better performance than OFDM, especially in high Doppler scenarios [17], [18].

1.4 Orthogonal Time Frequency Space Massive MIMO

5G networks aim to combine the benefits of massive MIMO and OTFS to increase spectrum efficiency, energy efficiency, data throughput, and reliable connection by implementing multi-user MIMO in high-Doppler scenarios. OTFS massive MIMO presents a low-complexity receiver design with ergodic capacity in high-Doppler scenarios [4]. Each OTFS massive MIMO system antenna transmits OTFS modulated information symbols independently.

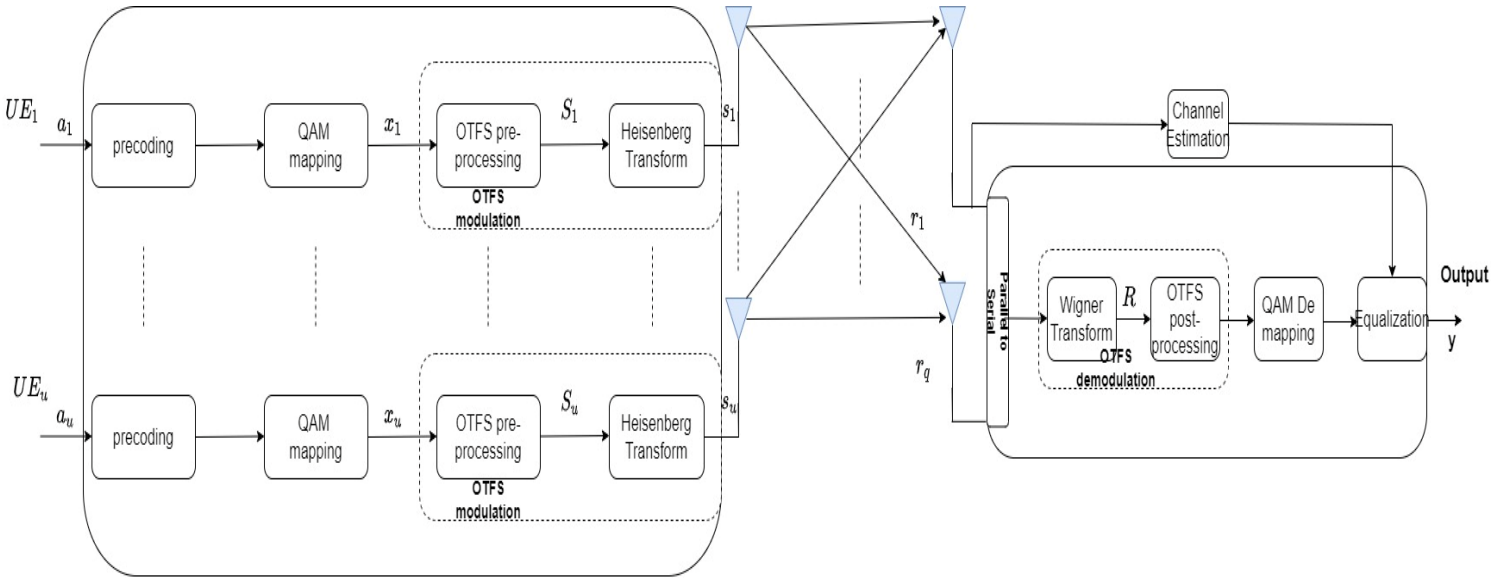

Figure 1.3: Uplink OTFS Massive MIMO modulation scheme

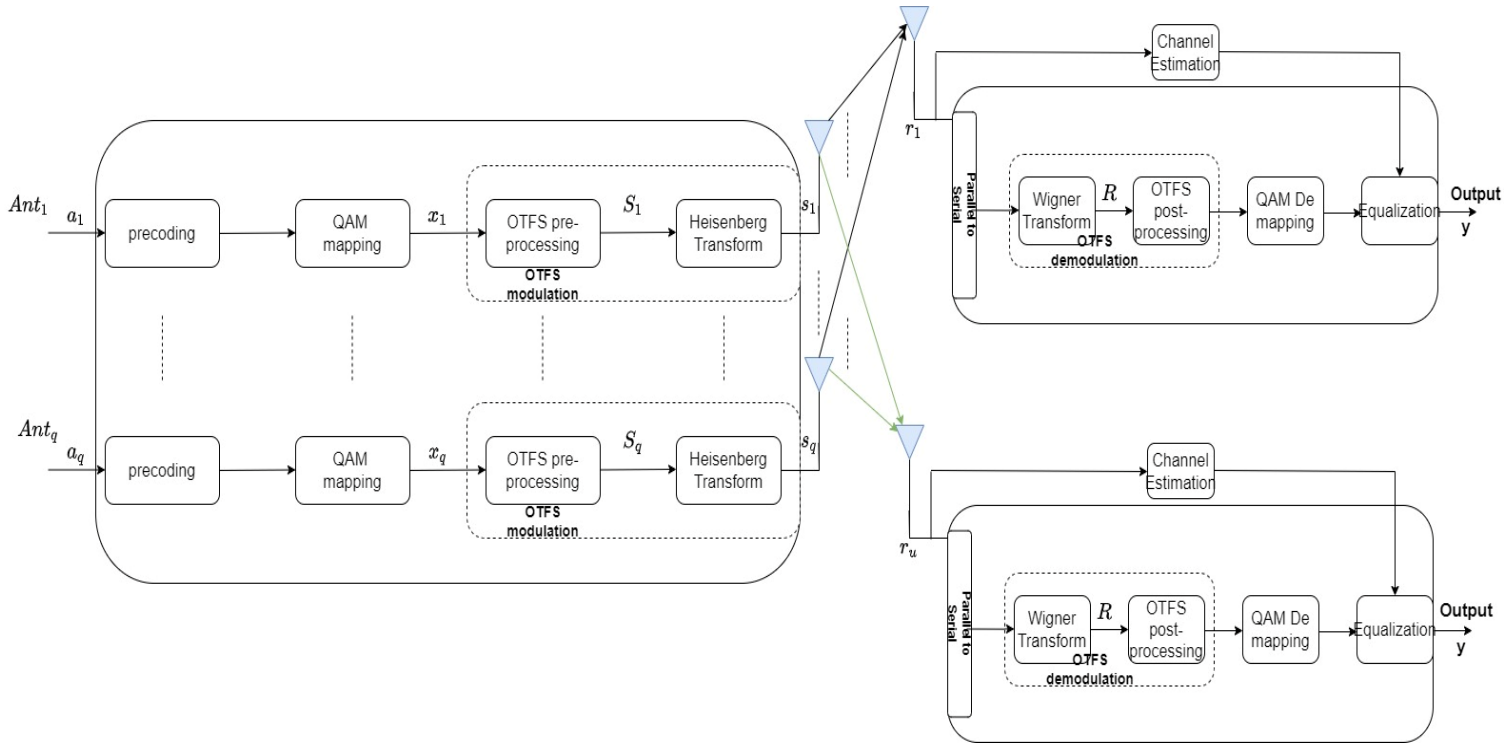

Figure 1.4: Downlink OTFS Massive MIMO modulation scheme

An OTFS massive MIMO system with a BS with q antennas which serves u $(q \gg u)$ single antenna UEs is considered as shown in Figure 1.3 and Figure 1.4. Precoding is performed to get rid of inter-user interference. For precoding, CSI of the transmitter is required, which is obtained by the receiver determining which pilot sequence each transmitter has transmitted [23]. Precoding will help make the system robust against channel order mismatch and zero

locations [24]. After precoding, the stream of bits goes through QAM mapping that yields the digitally mapped sequence of symbols and grouping of binary data [25]. The 2D transmit data block $\boldsymbol{x}$ in delay-Doppler is modulated through the OTFS modulation (ISFFT and transmitting windowing function as in Figure 1.2). The frequency-time domain signal goes through Heisenberg Transform, where the frequency-time domain is transformed into a time domain signal. CP is then added to the one-dimensional time-domain signal $\boldsymbol{s}$ to maintain orthogonality for all symbols between sub-carriers, simplify equalization at the receiver, and transmit the signals at the transmitter end. The time-domain received signal goes through CP removal and then parallel to serial conversion or demultiplexing. The demultiplexed one-dimensional signal $\boldsymbol{r}$ then goes through the Wigner Transform where the one-dimensional time-domain signal is transformed to the 2D frequency-time domain $\boldsymbol{R}$. The 2D frequency-time domain $\boldsymbol{R}$ then goes through OTFS post-processing where it will be transformed from frequency-time domain to 2D delay-Doppler and then goes through QAM demapping that gives binary data that was transmitted [26] and lastly equalization to remove impairments to give 2D delay-Doppler signal $\boldsymbol{y}$, which is compared to the transmitted signal, is carried out.

1.5 Research Focus

1.5.1 Introduction

This sub-section presents the works done in literature, problems addressed, and some of the new issues. This sub-section taps into some of the issues that need to be solved, formulated and motivates improvements. There is a presentation of the research question with its aims and objectives. Lastly, the procedure is formulated to realize the aims and objectives.

1.5.2 Motivation

The combination of OTFS and massive MIMO addresses the implementation and complexity of massive MIMO in 5G and future generation systems [10]. Good CSI allows the system to enjoy the benefits of OTFS and massive MIMO. Various channel estimation methods in high-Doppler scenarios have been presented in the literature. In [1], the OTFS channel estimation (CE) was expressed as a 2D structured Turbo-Compressive Sensing algorithm and in [5], [27], and [28] as a message-passing structured signal recovery problem. The increase in the number of channel paths of massive MIMO channels in high-Doppler scenarios, the implementation of the receiver in [1], [4], [5], and [27] might be too complicated to implement. Data-aided channel estimation for superimposed data and pilot transmission, a delay-Doppler domain

embedded pilot-based time-domain channel estimation for cyclic prefix-OTFS in the presence of residual frame timing offset, carrier frequency offset, and fractional multiple Doppler and pilot-aided channel estimation that is based on a threshold method were all implemented for OTFS-based systems in [29], [30] and [31], respectively. With the channel estimation in [29], [30], and [31] only reliant on transmitted symbols, it makes the interpolation techniques used for the detection process are not 100% accurate. It leads to high pilot overhead for OTFS massive MIMO transmission, which impairs the bandwidth efficiency of the system. In [17], three-dimensional structured orthogonal matching pursuit (3D-SOMP) algorithm-based downlink channel estimation technique was proposed, improving the transmission's pilot overhead performance. Expectation maximization based variational Bayesian (EM-VB) was implemented in [10] to estimate the uplink channel parameters in the time-domain OTFS massive MIMO. They implemented channel reciprocity to reconstruct the downlink channel parameters at the base station. As a result, low complex 3D channel estimation is obtained. However, the issue of pilot overhead and convergence rate is still a persistent problem in [10] and [17], especially in the presence of a massive number of antenna elements. This is mainly because the sparsity nature of the system in the angle domain means the channel estimation process will require more pilot symbols for the estimation of the angle domain supports.

As a result of the availability of CSI after the channel estimation process, the linear detection technique can be formulated to lower computational complexity cost and increase the possibility of a hardware implementation for OTFS massive MIMO. One of the ultimate research problems of OTFS-based massive MIMO systems is to develop computationally simple ways to detect transmitted data in many signals received. Good data detection allows the system to enjoy the benefits of the combination of OTFS and massive MIMO. Data detection aims to recover the transmitted data symbols. Data detection aims to recover the transmitted data symbols with a low error probability to have efficient transmission and reception of the original signal. Advanced and accurate detection schemes are required in OTFS massive MIMO systems because it gets challenging in high-Doppler scenarios in OTFS systems to keep track of the channel state information as it changes rapidly. Data detection of OTFS massive MIMO in high-Doppler scenarios is challenging because the channel parameters increase, complexity increases, and inter-carrier interference become very severe as mobile users rise.

Although non-linear detection methods like maximum a posteriori, sphere coding, K-best coding, and maximum likelihood exhibit optimal error performance, they are highly

computationally complex as the number of decision variables increases with the number of transmitted streams [32-33]. Emerging applications in communication systems require detectors to be less complex, have low computational latency, and have low computational area. As a result, that would lead to detectors with modest complexity being unacceptable because of stringent power and computational area constraints [32]. In [34], a linear-complexity detector was implemented for MIMO-OTFS based on maximum ratio combining (MRC) to efficiently connect the distinct antenna and multipath copies of the transmitted symbols and decrease the computational complexity. However, near-optimistic error performance, low complexity, and high-speed OTFS detectors are necessary to narrow the gap between algorithms and hardware implementation. In [35], there was an implementation of the Gauss-Seidel (GS) based MRC for single input single output (SISO)-OTFS over-relaxation parameter in the rake detector to better the performance and the convergence speed of the iterative detection. In [17], low complexity minimum mean square error (MMSE) detection was used in the OTFS system to balance the trade-off between complexity and optimal performance. However, detection methods like zero-forcing (ZF) and MMSE involve matrix inversion in the massive MIMO systems; they become undesirable because they increase the detection process's complexity [36]. To tackle the problem of matrix inversion in the OTFS massive MIMO system introduced by MMSE and reduce the complexity of data detection, a less complex Neumann Series Expansion (NSE) soft detection is proposed MMSE method [37]. NSE finds the necessary matrix inverse at low complexity. As much as NSE reduces the complexity of MMSE detection, a small reduction in complexity cost is achieved in implementing NSE. To further accelerate the convergence and further reduce the complexity of MMSE detection, there is a need to propose a new detection method in OTFS massive MIMO, which has a performance much closer to that of the typical MMSE detection method [32],[38]. Thus, eventually making detection at the receiver for OTFS massive MIMO has more straightforward hardware implementation [32].

1.5.3 Research Question

The apparent need for improvement of CE for OTFS massive MIMO by a decrease in computational complexity and decrease in pilot overhead by exploiting the sparsity nature of OTFS massive MIMO, the need for improvement of data detection by lowering computational complexity cost of MMSE data detection and approaching optimal performance and the desire to improve the receiver's performance by joint CE and data detection is the foundation of the following question:

To what extent do compressive sensing channel estimation techniques and linear data detection techniques in the delay-Doppler domain improve the efficiency of the OTFS-massive MIMO channel estimation scheme in terms of NMSE, BER, computational complexity cost, and pilot overhead ratio?

To undertake the above main question, the following questions were addressed as they led to the answer that solved some of the problems presented in the literature:

- What compressive sensing algorithm (s) can be employed with interleaving for the CE scheme to improve the efficiency of the OTFS-massive MIMO systems?
- How can the CE schemes that exhibit improved performance and low computational complexities be developed for OTFS-massive MIMO systems?
- How can a data detection scheme that will improve the data recovery performance in OTFS-massive MIMO systems be developed as a linear algorithm?

1.5.4 Aims and Objectives

This research aims at developing a low complexity linear detection technique and compressive sensing-based channel estimation techniques to better the efficiency of OTFS massive MIMO that guarantees better error performance, less pilot overhead, minimum implementation complexity, and eventually economical in real-world applications.

The objectives of this research are as follows:

- Development of an algorithm that takes advantage of the sparse nature of the OTFS-massive MIMO in high-Doppler scenarios and implement the technique to obtain CE of OTFS massive MIMO in high-Doppler scenarios.
- Development of a low complex linear detection scheme for OTFS massive MIMO system which allows for it to be used in less powerful/low-cost hardware.

Considering all the aforementioned proposed channel estimation techniques in the literature for OTFS massive MIMO system, it is necessary to develop new channel estimation schemes. Such schemes are expected to have better reconstruction performances and require low pilot overhead for channel estimation procedures in high-Doppler scenarios.

It is necessary to develop a new data detection scheme considering all the aforementioned proposed data detection schemes in the literature for the OTFS massive MIMO system. The proposed method is expected to have almost optimal performance and low computational complexity, making hardware implementation easier and converging quicker.

1.6 Publications

The following journal papers have resulted from this research,

- Rodwell Muzavazi and Olutayo O. Oyerinde, "Delay-Doppler Subspace Pursuit based channel estimation scheme for OTFS-massive MIMO System," *Springer Telecommunication Systems 2021, under review*.
- Rodwell Muzavazi and Olutayo O. Oyerinde, "Channel Estimation and Data Detection Scheme for Downlink and Uplink OTFS massive MIMO Systems," *Elsevier Computers and Electrical Engineering 2022, accepted*.

1.7 Dissertation Organization

The rest of the dissertation is organized as follows:

Chapter 2: Chapter 2 provides the background of the literature on channel estimation, OTFS, OTFS massive MIMO channel estimation and detection for OTFS massive MIMO systems. The downlink system model for OTFS massive MIMO and the uplink system model for OTFS massive MIMO system are also introduced.

Chapter 3: This chapter presents the proposed compressive sensing channel estimation method and the channel estimation algorithm with the interleaving technique. The performances of the system are analyzed and discussed in terms of NMSE.

Chapter 4: This chapter presents the proposed delay-Doppler compressive sensing channel estimation scheme and the channel estimation algorithm. The performances of the system are analyzed and discussed in terms of NMSE.

Chapter 5: Chapter 5 presents the derivation of the proposed detection technique, and the data detection algorithm is introduced. The system's performances are analyzed and discussed in terms of BER and the number of complex multiplications.

Chapter 6: Finally, this chapter draws the curtains on the dissertation and presents the summary of contributions of this research. This part further summarizes all the obtained results and how they contribute to the betterment of future generation networks.

Chapter 2 - Literature Review – Channel Estimation and Data Detection for OTFS Massive MIMO

2.1 Introduction

This chapter presents literature documented so far concerning channel estimation and data detection. The goal is to pave the way for the proposed channel estimation and data detection schemes to close the literature gaps for OTFS massive MIMO systems. Initially, a survey on channel estimation and data detection techniques is presented. As a result, that allows the research to focus on the channel estimation technique that answers some of the unanswered questions in literature for OTFS massive MIMO systems. This chapter also explores channel estimation and data detection in massive MIMO, which eventually leads to formulating the channel estimation and data detection techniques for OTFS massive MIMO. Finally, the investigation is concluded by formulating a downlink system model for channel estimation for OTFS massive MIMO and an uplink system model for data detection for OTFS massive MIMO. The developed models help to improve hardware implementation, error performance, computational complexity, and pilot overhead ratio.

2.2 Channel Models

Mobile communication systems are severely reliant on channel models. The channel impulse response (CIR) characterizes the complex channel and gives information crucial to scrutinize the transmitted signals [39]. There are two types of channel models named: deterministic and stochastic. Modeling of designing parameters for conformity testing of wireless communication systems is deterministic modeling. Stochastic models are usually fitted for generating random channel realizations for scrutinizing and testing how a system performs at the system level or link level. These stochastic models are determined by initially estimating the channel parameters, e.g., Doppler frequency spread, delay spread and the parameters of individual propagation paths from individual channel snapshots and determining the channel parameters' statistics for modeling [39]. According to [39], $x(t)$ is the transmitted signal in the wireless communication channel, $s(t)$ is the complex signal equivalent to the message signal, and $2\pi f_c$ is equal to the carrier frequency of the modulator as:

$$x(t) = \mathrm{Re}\{\left(s(t)e^{j2\pi f_c t}\right)\}. \tag{2.1}$$

According to [39], $a_m(t)$, $\tau_m(t)$, and M are time-dependent complex amplitude, time-dependent delay associated with *m*th path, and the number of paths, respectively as:

$$r(t) = \sum_{m=0}^{M-1} a_m(t)x(t - \tau_m(t)). \quad (2.2)$$

2.3 Channel Estimation Techniques

A good CSI because of good CE guarantees accurate recovery of the transmitted signal at the receiver. Good CE is measured by how accurate the system can predict the effects of the propagation channel. The unwanted effects of the wireless communication system caused by the physical properties of the channel lead to the distortion of the received signal. The receiving power of the system is complexly influenced by fading, shadowing, reflection, refraction, scattering and diffraction.

As a result of all the propagation loss experienced in the wireless communication system's environment, the propagated signal is exposed to path loss, multi-path fading, time spread, and Doppler frequency shift. The phase and amplitude of the combination of signals will determine the phase and amplitude of the received signal. Due to the magnitudes of the phases of the components, the combined effect of the components may strengthen or weaken the amplitude of the combined signal. There is a possibility that the two combined signals may cancel each other depending on their relative phases on their amplitudes. The received signal weakening due to the combined signals' destructive interference is called fading [39]. In wireless communication systems, we have large-scale fading and small-scale fading. Large-scale fading is due to the general terrain (landform or geographic) and the density and height of buildings. Large-scale fading is characterized statistically by the mean path loss and lognormal shadowing, and it varies relatively slow with time. Large-scale fading predicts behavior averaged over distances more significant than the wavelength, and it is crucial for anticipating the coverage and availability of a service.

On the other hand, small-scale fading is caused by the local environment, that is, trees, buildings, and the movement of the radio terminal through the atmosphere. Small-scale fading has a shorter timescale and has been characterized statistically by fast Rayleigh fading because of multi-path and lack of line-of-sight signal [39]. On the other hand, if the small-scale fading has a dominant non-fading component and a line-of-sight propagation, it is called Rician fading [39]. Small-scale fading sheds light on the signal variability on a wavelength scale, and it is crucial for designing the modulation format and general transmitter and receiver.

Recovering the optimal CSI is still one of the biggest hindrances of a great performing wireless communication. If the receiver fails to predict the channel perfectly, the transmitted signal will be demodulated and detected with a significant loss in signal-noise-ratio (SNR) [39]. The development of CE techniques that will produce CSI for coherent detection at the receiver should be explored [39] to minimize the losses of the transmitted signal and provide good quality of service (QoS) in wireless communication systems.

CE analyses or predicts the statistics of the wireless channel and gets the measure the channel impacts on the transmitted signal. This approximation of the effect of the channel on the transmitted signal improves the wireless communication system performance [26]. The biggest challenge for wireless communication systems is to provide a perfect CSI that is accurate and up to date. The correct and updated CSI leads to accurate signal demodulation, equalization, decoding, and other signal applications. Also, distortion of the transmitted signal when it passes through the wireless channel will mean the received signal needs channel equalization to maintain orthogonality, which also helps to nullify the impairments of the frequency selective fading environments [40].

Accomplishing reliable communications in wireless communication systems, including robust and accurate CSI, is paramount. Researchers have spent a vast amount of time developing efficient CE techniques for many unique transmission and modulation schemes [41]. CE techniques are pilot-assisted (training-based) channel estimation, blind and semi-blind channel estimation, and decision-directed channel estimation.

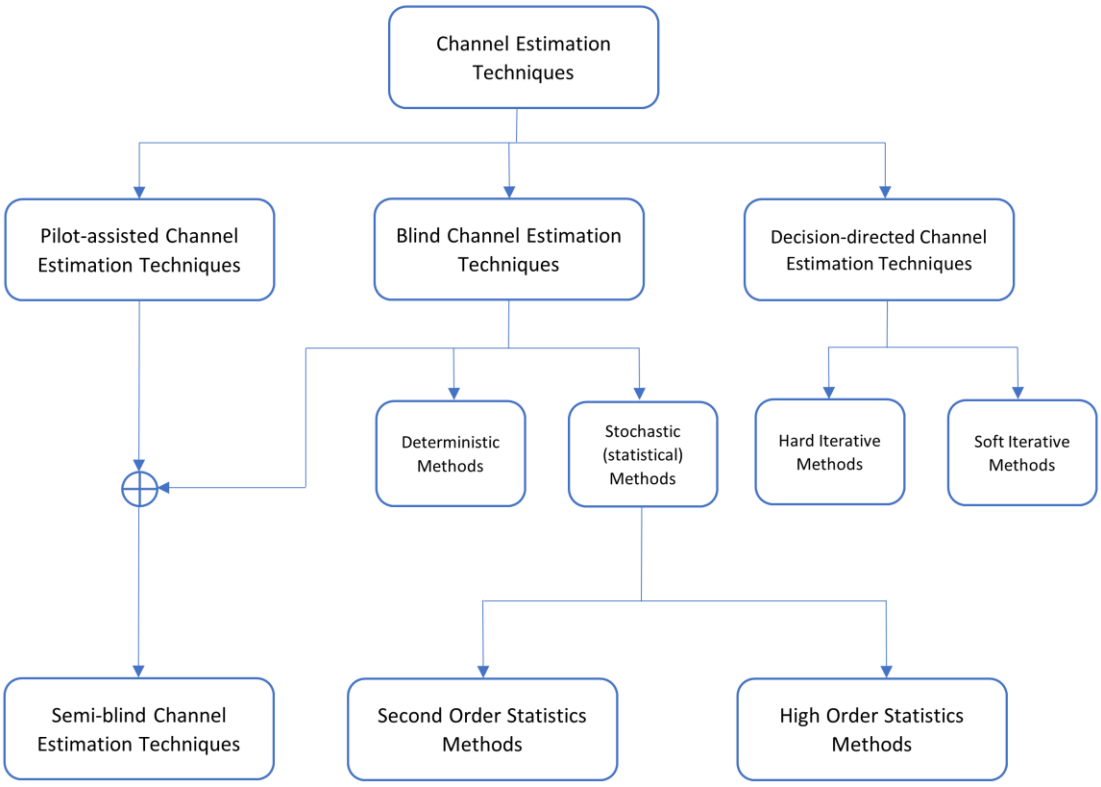

Figure 2.1: Classifications of Channel Estimation Techniques [39]

2.3.1 Pilot-assisted Channel Estimation (PACE)

PACE technique also referred to as the training-based CE scheme, is a common way of obtaining the characteristics of the channel in wireless communication systems. Training symbols are first transmitted for CE, and the data symbols are obtained by interpolating the CSI received via pilot signals. Equalization detection is performed using the CSI estimated by the pilot signals in the PACE technique [42]. Interpolation at the receiver is applied to estimate the channel transfer function in the whole bandwidth. PACE is usually applied in frequency selective channels [43]. The training signal should be transmitted as soon as the fading condition in the wireless communication system is changed. In fast fading conditions, the amount of data symbols transmitted is reduced due to the high transmission of training signals [44]. PACE also introduces unresolved errors into the estimation process because they make CEs only depend on the training symbols and the interpolation techniques used, as expected, can never be 100% [39]. Some of the existing PACE methods include least-squares (LS), ML, and MMSE, which are usually used in many CE estimation techniques to enhance the CE

technique, e.g., in [45], the MMSE was used to equalize the channel and split users' data, and the few randomly chosen algorithms are generalized below.

According to [42], in a point-to-point wireless communication system, the CE model can be described as:

$$y = xh + n, \tag{2.3}$$

where y is the received signal during the training period, x are the training symbols transmitted in the wireless communication system, h is the unknown channel of the system to be determined, and n is the unknown AWGN.

2.3.1.1 Least Squares Channel Estimation (LSCE)

LSCE is usually used indoors where the environment is relatively stationary. In a general case with no statistical knowledge of the noise n [42], estimation of the channel can be carried out using LSCE. LSCE aims to guarantee a minimum square norm between y in (2.3) and the zero-noise data:

$$\hat{\mathbf{h}}_{LS} = \min_{\boldsymbol{h}} \underbrace{\|\boldsymbol{y} - \boldsymbol{xh}\|^2}_{J_{LS}}, \tag{2.4}$$

where J_{LS} is the cost function of the LSCE. After differentiating J_{LS} with respect to $\boldsymbol{h}$. Equating the derivative to zero yields LSCE:

$$\hat{\mathbf{h}}_{LS} = (x^H x)^{-1} x^H y. \tag{2.5}$$

It is worth noting that LSCE severely deteriorates performance in high mobility scenarios [41].

2.3.1.2 Maximum-Likelihood Channel Estimation (MLCE)

The likelihood function is the probability density function (PDF) of y conditioned on $\boldsymbol{h}$ [42]. The likelihood function shows us how possible a certain y is observed with a given $\boldsymbol{h}$ as:

$$\hat{\mathbf{h}}_{ML} = arg \min_{\boldsymbol{h}} p(\boldsymbol{y}|\boldsymbol{h}). \tag{2.6}$$

Generally, covariance is part of the experimental design that shows how noise affects the general data of a model estimate. If the noise in the channel is assumed to be Gaussian with covariance $\mathbf{C_n}$ like in (2.3), then $p(\boldsymbol{y}|\boldsymbol{h})$ is:

$$p(\boldsymbol{y}|\boldsymbol{h}) = \frac{1}{|\pi \mathbf{C_n}|} exp\big[(\boldsymbol{y} - \boldsymbol{xh})^{\boldsymbol{H}} \mathbf{C_n}^{-1} (\boldsymbol{y} - \boldsymbol{xh})\big]. \tag{2.7}$$

From the derivation of the function in (2.6), the MLCE of $\boldsymbol{h}$ can be derived as:

$$\hat{\mathbf{h}}_{ML} = \arg \min_{\boldsymbol{h}} \underbrace{(\boldsymbol{y} - \boldsymbol{xh})^{H} \mathbf{C_n}^{-1} (\boldsymbol{y} - \boldsymbol{xh})}_{J_{ML}}. \tag{2.8}$$

Equating the derivation of J_{ML} to zero will yield:

$$\hat{\mathbf{h}}_{ML} = (\boldsymbol{x}^{H} \mathbf{C}_n^{-1} \boldsymbol{x})^{-1} \boldsymbol{x}^{H} \mathbf{C_n}^{-1} \boldsymbol{y}. \tag{2.9}$$

Assuming white noise in the channel, the maximum estimation error is:

$$\boldsymbol{h}_{MSE} = (\boldsymbol{x}^{H} \mathbf{C}_n^{-1} \boldsymbol{x})^{-1}. \tag{2.10}$$

2.3.1.3 Minimum Mean Square Error Channel Estimation (MMSECE)

If $\boldsymbol{h}$ is assumed to be a random vector and the statistics are known as PDF, then the communication system can rely on the statistics to improve the accuracy of the CE. In [42] the MMSECE is then defined as:

$$\boldsymbol{h}_{MMSE} = \arg\min_{\boldsymbol{h}}\{(\boldsymbol{h}-\widehat{\boldsymbol{h}})^{H}(\boldsymbol{h}-\widehat{\boldsymbol{h}})\}. \tag{2.11}$$

If $\boldsymbol{h}$ is assumed to have mean $\boldsymbol{\mu}$ and covariance $\mathbf{C}_h$, (2.11) can be further simplified to

$$\boldsymbol{h}_{MMSE} = \boldsymbol{\mu}_h + (\boldsymbol{C_h}^{-1} + \boldsymbol{x}^{H}\boldsymbol{C_n}^{-1}\boldsymbol{x})^{-1}\boldsymbol{C_n}^{-1}(\boldsymbol{y}-\boldsymbol{x}\boldsymbol{\mu_h}). \tag{2.12}$$

2.3.2 Blind Channel Estimation (BCE)

One of the most significant setbacks for PACE is bandwidth wastage. Pilot symbols will occupy parts of the bandwidth that data signals could have occupied. Moreover, the time consumed by sending and estimating the training symbols before the data symbols can be transmitted induces latency in the wireless communication system. Applications like data transmission, reverberation cancellation, and image deblurring use BCE. BCE arises in the frequency selective fading scenarios because training symbols are unavailable. In BCE, the training signals are avoided, increasing the bandwidth efficiency (BE) [42]. On the other hand, BCE exhibits a slow convergence rate, and this is because of the inherent limitations caused by BCE's random-like search mechanisms. As a result, making BCE is tough to implement in a practical system [46]. BCE can be very effective if the underlying multipath channel remains constant over many multipath OFDM signals [47].

Semi-blind channel estimation (SBCE) combines PACE and BCE methods [39]. In the SBCE technique, inherent information about the unknown transmitted signal and information about the known pilot symbols are applied for CE. The few pilot signals combined with the BCE solve the convergence problems experienced by BCE [48]. SBCE is considered a practical

solution for practical wireless systems because it gives better CE accuracy and BE [49]. On the other hand, SBCE uses a vast amount of processing operations and optimization of the CE is needed to keep the computational complexity at a minimum in SBCE [50].

BCE algorithms use second-order statistics (SOS) or correlation matrix [51], correlative coding, and other properties usually have better BE. The cyclic statistics characteristics of the received signals are BCE statistical methods. In deterministic BCE methods, the statistic characteristics of the received signals are not used, and the channel coefficients and received signals are both considered deterministic quantities [39]. Most SOS BCE identify the entire discrete channel, including the pulse shaping and receiver filters [52]. A vast number of the blind and semi-blind MIMO-OFDM CE techniques in the literature implement second-order statistics [49]. CE using SOS requires a smaller data length and will give smaller variance estimation [53]. However, these techniques need many OFDM symbols to predict the correlation matrix reliably, making them unsuitable and cumbersome for fast-varying channels. A fast-varying channel varies faster than the baud rate [49],[54]. Deterministic BCE converges quicker than statistical CE but at the expense of higher computational complexity cost [39]. It is also essential to note that the correct channel order for BCE and equalization is significant [55].

2.3.3 Decision-directed Channel Estimation (DDCE)

DDCE provides a more reliable CE than PACE because it implements training symbols and re-modulates detected message symbols [39]. DDCE implements fewer training symbols compared to PACE in the absence of errors. In DDCE, the initial *posteriori* channel transfer function is employed in CE during the demodulation stage of the successive symbols received in the next time slot. The detector or equaliser calculates soft or hard symbol information and feeds back to better the quality of CE as the magnitude of iterations increases [39].

2.4 OTFS Channel Estimation

OTFS is considered to replace OFDM in 5G and future generation systems due to an increase in BE and better performance in high Doppler scenarios, amongst other positives presented by OTFS. The fast-varying channels in the high-speed mobility channel will degrade the OFDM performance if the Doppler effect is not compensated accurately. Due to the assumption that an almost linear time-invariant (LTI) channel in OTFS, which is a result of geometric properties

of the channel changes more slowly (quasi-static) over time. OTFS allows the system to measure the channel in a longer observation time than OFDM in high Doppler scenarios [1]. Due to the quasi-static nature of the OTFS, it makes CE much easier. In OFDM [56], the frequency domain is usually where the estimation of the selected subcarriers is done, and the observations are utilized to interpolate the rest of the subcarriers. The channel estimation in OTFS is done in the delay-Doppler domain, which is in 2D, compared to OFDM, which is generally in 1D, i.e., symbols in OTFS are usually scattered in the time and frequency domain (doubly dispersive). The receiver utilizes pilot symbols transmitted in the delay-Doppler domain in OTFS [17].

2.5 Massive MIMO Channel Estimation

Massive MIMO extends the existing MIMO technology in 4G, LTE, and 3GPP. Massive MIMO harvests the benefits of MIMO on a massive scale. However, to reap the benefits, accurate CSI is required. Coherent detection in massive MIMO is possible when reliable CE is computed. One of the most significant setbacks of the massive MIMO is the increase of the complexity of CE by the increase in the number of antennas, and sometimes the increase in the receive antennas leads to the reduction of CE accuracy. As a result, that makes CE in massive MIMO very difficult. Future-generation wireless systems need more techniques to guarantee high BE [57], high throughput and accommodate many users in one cell, and massive MIMO is the answer.

Under the standard methods of CE in MIMO, pilot overhead is directly proportional to the increase in the number of antennas [58]. The issue of high pilot overhead is a severe threat to the efficiency of massive MIMO technology in future generation wireless communications, which has led to researchers exploring blind and semi-blind CE in massive MIMO. On a larger scale, the most common algorithms for MIMO CE are pilot-assisted, blind, and semi-blind estimators [59]. BCE will perform better than PACE in a massive MIMO system because BCE does not rely on the training sequence but the channel's natural constraints [60]. Massive MIMO CIRs, empirically and theoretically, demonstrate joint spatial sparsity that remains almost unchanged within the coherence time because of the temporal correlation of channels due to finite significant scatters and the compact standard BS antenna array [61]. This channel sparsity in massive MIMO is advantageous for designing the system because it can be exploited to design more efficient CE techniques [56]. As a result, the number of null coefficients of the channel is minimal compared to the channel length. Then, estimation of the wireless channel

can be done by the CS technique. CS algorithms can be divided into three main groups: convex relaxation, Bayesian interference, and greedy iterative algorithms [23]. The CS problem can be computed as a convex optimization in complex convex relaxation algorithms like basis pursuit (BP) and BP de-noising (BPDN). The minimization of the cost function, where the expectation is taken about the unknown channel parameters conditioned on the received training sequence, is done by Bayesian interference algorithms [62]. On the other hand, greedy iterative algorithms identify the support set of the null elements in a simple and less complex greedy iterative manner [23]. The literature in CS can provide accurate CE using a relatively small number of training tones if the training symbols are selected randomly [47].

2.6 OTFS Massive MIMO Channel Estimation

The high mobility in the transmitter or receiver will cause the channels to vary with time, i.e., the channel experiences time-selective fading [10]. Some works were done in literature to mitigate that shortcoming experienced when implementing massive MIMO systems. In [63], angle domain Doppler compensation application for high-speed wideband massive MIMO in uplink communications was implemented. In [63], high-mobility Coordinated Multi-Point Uplink transmission, where a high-speed terminal of a high-speed train simultaneously sends signals to multiple BSs with angle-domain Doppler shifts compensation. Derivation of the exact Power Spectrum Density (PSD) for uplink from a high-speed railway to BS was explored for consideration. In addition, further reduction of the channel time variation via beamforming network optimization is proposed. The work in [64] considers a Doppler compensation technique for a linear precoder in massive MIMO. In [65], analysis of the performance of UEs in groups and scheduling in high-mobility scenarios is investigated and the approach used reduces the precoding transmit antenna size. However, OFDM's massive MIMO degrades enormously in high mobility scenarios. On the other hand, the OTFS outperforms OFDM in high-speed scenarios, and massive MIMO in combination with the OTFS technique can support very high throughput and performance links and BE by serving several spatially separated users simultaneously in the same resource block. In [15], a 3D-SOMP algorithm-based CE technique was proposed. The 3D-SOMP in [15] reduces pilot overhead in downlink OTFS massive MIMO under high-Doppler scenarios. In [10], the work explores the massive MIMO-OTFS signal model's time domain in high-speed systems. In [10], the uplink channel parameters, including angle, delay, the Doppler frequency; and channel gain for each physical scattering path are recovered. Then they are used for exploitation of the angle, delay, and Doppler

reciprocity between uplink and the downlink and use those parameters to reconstruct the angles, delays, and Doppler frequencies for the downlink channels at the BS.

2.6.1 Formulation of the Downlink OTFS Massive MIMO Channel Estimation Model

Figure 1.4 shows an OTFS massive MIMO scheme with a base station with *q* antennas which serves *u* single antenna user equipment. Downlink precoding makes the system more robust against channel order mismatch and zero locations [24]. After precoding, the stream bits go through QAM mapping that yields the digitally mapped sequence symbols and grouping of binary data [25]. The 2D transmit data block $\boldsymbol{x}$ is modulated through OTFS modulation (ISFFT and transmitting windowing function) in the delay-Doppler domain. The frequency-time domain $\boldsymbol{S}$ goes through Heisenberg Transform to the time domain $\boldsymbol{s}$. Cyclic prefix symbols are added to the one-dimensional time-domain signal $\boldsymbol{s}$ to maintain orthogonality for all symbols between subcarriers and transmitted towards the user equipment. At the receiver, the time domain signal received $\boldsymbol{r}$ is initially freed of the cyclic prefix symbols and then goes through parallel to serial conversion or demultiplexing. The demultiplexed one-dimensional signal then goes through the Wigner transform, where it is transformed to a 2D time-frequency domain $\boldsymbol{R}$. The 2D frequency-time domain $\boldsymbol{R}$ then goes through OTFS post-processing, where it will be transformed from frequency-time domain to 2D delay-Doppler and then goes through QAM demapping that gives binary data that was transmitted [26]. Lastly, equalization to remove impairments in the transmitted signal to result in 2D delay-Doppler signal $\boldsymbol{y}$ is performed.

The output signal in the delay-Doppler domain at the receiver is represented by $\boldsymbol{y}$ in the system model in Figure 1.4. For the *q*th base station antenna, the received signal is

$$\boldsymbol{y}^q = \boldsymbol{H}^q \boldsymbol{d}^q + \boldsymbol{v}^q, \tag{2.13}$$

where H^q is the *q*th base station antenna's delay-Doppler channel gain matrix, $\boldsymbol{v}^q$ represents the *q*th antenna's additive white Gaussian noise (AWGN) occurred in the whole channel with zero mean and covariance matrix of $\sigma^2 \boldsymbol{I}_u$ because that makes noise experienced by each UE different, and $\boldsymbol{d}^q$ represents the transmitted symbol vector of the *q*th base station antenna information transmitted $\boldsymbol{a}$,

$$\boldsymbol{d}^q = \boldsymbol{V}^q \boldsymbol{a}^q, \tag{2.14}$$

where $\boldsymbol{V}$ is the precoding matrix. If data matrices of all antennas are stacked up to form a $Mq \times N$ matrix $\boldsymbol{B}$ as:

$$\boldsymbol{B} = \begin{bmatrix} \boldsymbol{D}^0 \\ \boldsymbol{D}^1 \\ \vdots \\ \boldsymbol{D}^{q-1} \end{bmatrix}, \tag{2.15}$$

where $\boldsymbol{D}^q$ is the 2D complex $M \times N$ data matrix of the qth base station antenna. After *ISFFT* to each sub-matrix $\boldsymbol{D}^q$,

$$\boldsymbol{X} = (\boldsymbol{I}_q \otimes \boldsymbol{F}_M)\boldsymbol{B}{\boldsymbol{F}_N}^H. \tag{2.16}$$

$\boldsymbol{x}$ is the vectorized version of $\boldsymbol{B}$ according to Figure 1.2, defined as follows:

$$\boldsymbol{x} = \begin{bmatrix} b_0 \\ b_1 \\ \vdots \\ b_{N-1} \end{bmatrix}, \qquad \boldsymbol{b}_n = \begin{bmatrix} {\boldsymbol{b}_n}^0 \\ {\boldsymbol{b}_n}^1 \\ \vdots \\ {\boldsymbol{b}_n}^{q-1} \end{bmatrix}, \qquad {\boldsymbol{b}_n}^j = \begin{bmatrix} {\boldsymbol{b}_{0,n}}^0 \\ {\boldsymbol{b}_{1,n}}^1 \\ \vdots \\ {\boldsymbol{b}_{M-1,n}}^{q-1} \end{bmatrix}, \tag{2.17}$$

where ${\boldsymbol{b}_{m,n}}^j$ is the data symbol of the jth transmitting base station antenna and $j = 0,1, \dots, q-1$. According to [4],

$$\overline{\boldsymbol{X}} = ({\boldsymbol{F}_N}^H \otimes \boldsymbol{I}_q \otimes \boldsymbol{F}_M)\boldsymbol{x}. \tag{2.18}$$

After partitioning $\bar{\boldsymbol{X}}$ to N blocks, $\bar{\boldsymbol{X}}_n$, the transmit windowing function is multiplied by each block. The windowing function works in combination with the bi-orthogonality property, which aims to eliminate ISI. In [21], it is shown that the windowing function also induces a reduction in OoB radiation and an increase in peak to average power (PAPR). If all base station antennas are considered to use the same windowing function, then the time-frequency domain signal $\boldsymbol{S}_n$ after the windowing function is:

$$\boldsymbol{S}_n = \bar{\boldsymbol{K}}_n \bar{\boldsymbol{X}}_n, \tag{2.19}$$

where $\bar{\boldsymbol{K}}_n = \boldsymbol{I}_q \otimes \boldsymbol{K}_n$, K_n is the nth $\boldsymbol{W}^{tx}$ (transmit windowing matrix) in (2.18).

The Heisenberg Transform in Figure 1.3, which is part of the OTFS modulation in Figure 1.2, will transform the frequency-time domain signal of each base station antenna to the time-domain as:

$$\boldsymbol{s}_n = (\boldsymbol{I}_q \otimes {\boldsymbol{F}_M}^H)\boldsymbol{S}_n, \tag{2.20}$$

$$\boldsymbol{s} = \left(\boldsymbol{I}_{Nq} \otimes {\boldsymbol{F}_M}^H\right)\boldsymbol{S}. \tag{2.21}$$

The transmitter will add cyclic prefix symbols to the signal in the time domain to be transmitted and send the signal through the channel. The multipath propagation of the OFDM symbols introduces overlapping of the adjacent symbols and, as a result, gives rise to ISI, which lowers the performance of the OFDM. As a result, the Heisenberg transform uses the cyclic prefix to better the performance of the OFDM. The cyclic prefix length should exceed the maximum delay of the multipath propagation channel. The transmitted signal becomes periodic due to the cyclic prefix. Moreover, the effect of the time-dispersive multipath channel becomes equivalent to a cyclic convolution. The receiver will first remove the cyclic prefix, and after the received signal is cyclic prefix-free, it can be written as:

$$\boldsymbol{r}_n = (\boldsymbol{I}_u \otimes \boldsymbol{R}_{CP})\boldsymbol{H}_n\left(\boldsymbol{I}_q \otimes \boldsymbol{A}_{CP}\right)\boldsymbol{s}_n + \boldsymbol{v}_n$$

$$= \bar{\boldsymbol{H}}_n \boldsymbol{s}_n + \boldsymbol{v}_n, \tag{2.22}$$

$$\bar{\boldsymbol{H}}_n = \begin{bmatrix} \bar{\boldsymbol{H}}_n^{\,0,0} & \bar{\boldsymbol{H}}_n^{\,0,1} & \cdots & \bar{\boldsymbol{H}}_n^{\,0,q-1} \\ \bar{\boldsymbol{H}}_n^{\,1,0} & \bar{\boldsymbol{H}}_n^{\,1,1} & & \bar{\boldsymbol{H}}_n^{\,1,q-1} \\ \vdots & & \ddots & \vdots \\ \bar{\boldsymbol{H}}_n^{\,u-1,0} & \bar{\boldsymbol{H}}_n^{\,u-1,1} & \cdots & \bar{\boldsymbol{H}}_n^{\,u-1,q-1} \end{bmatrix}. \tag{2.23}$$

$\bar{\boldsymbol{H}}_n^{\,u,j}$ is the nth CIR matrix between jth base station antenna and uth user equipment. As a result, according to Figure 1.2,

$$\boldsymbol{r} = \bar{\boldsymbol{H}}\boldsymbol{s} + \boldsymbol{v}, \tag{2.24}$$

where $\bar{H}$ is $diag\{\bar{\boldsymbol{H}}_n\}$. When the transmitted signal is received, the cyclic prefix symbols are removed first, and then the signal goes through *DFT*. The output of the Wigner Transform according to Figure 1.2 will be

$$\bar{\boldsymbol{r}} = (\boldsymbol{I}_{Nu} \otimes \boldsymbol{F}_M)\boldsymbol{r}, \tag{2.25}$$

$\bar{\boldsymbol{r}}$ is the length MNu frequency-time signal vector. Introducing the cyclic prefix preceding each symbol helps equalization and makes it more straightforward in computational complexity. However, the CIR should not exceed the cyclic prefix length for the equalization of each subcarrier to have less computational complexity. The cyclic prefix does not carry useful information. The cyclic prefix is kept as short as possible, implying that often the CIR length exceeds the cyclic prefix. The result of the length of the CIR exceeding the length of the cyclic prefix leads to poor performance because of ICI. The receiving windowing function reduces the spectral leakage effect due to the spectrum occupied by the transmitter and receiver in high Doppler scenarios. The receiver is more spectrally contained by reducing OoB due to the receiver windowing. After the signal is multiplied by the receiving windowing function, it gets

mapped with the delay-Doppler domain, and the estimation of the transmitted signal can finally be obtained as

$$\boldsymbol{y} = (\boldsymbol{F}_N \otimes \boldsymbol{I}_u \otimes \boldsymbol{F}_M{}^H)\boldsymbol{Y}, \tag{2.26}$$

where $\boldsymbol{Y}_m = \bar{\boldsymbol{P}}_m \boldsymbol{R}_m$, $\bar{\boldsymbol{P}}_m = \boldsymbol{I}_u \otimes \boldsymbol{P}_m$, $\boldsymbol{P}_m$ is the mth $\boldsymbol{W}^{rx}$ (receive windowing matrix). Using equations (2.13) to equation (2.26), it is easier to formulate a relationship to obtain the estimation of the channel and the transmitted signal. However, most of the existing channel estimation techniques in the literature are difficult to implement directly for OTFS massive MIMO systems because of the massive number of antennas involved [17]. The massive number of antennas is directly proportional to the number of transmitting orthogonal pilots, which causes high pilot overhead.

2.7 Detection of transmitted signals in Massive MIMO

Detection of massive MIMO aims at recovering transmitted symbols. The detection should have the minimum possibility of error by utilizing the minimum level of precision in the receiver using unique decomposition schemes [66]. For accurate detection in massive MIMO, advanced signal processing techniques are needed. Signal detection implies an accurate channel estimation of the transmit vector, knowing the received vector and the channel [12]. There are two types of detection algorithms: linear detection and non-linear detection. There is a trade-off between low complexity and poor performance in linear detection [67]. Minimum-complexity massive MIMO applies detection based on probabilistic data association [12]. The performance quality decreases due to the number of transmitting antennas increases in linear detection. However, in non-linear detection like maximum likelihood, the algorithms approach optimal levels yet pose high complexity, huge problem size, and lack of knowledge of the problem structure. The high dimensions of data detection experienced in uplink will give rise to excessively high computational complexity at the BS [68]. As a result, this research explores linear data detection for OTFS massive MIMO. However, matrix inversion of high dimensional matrices for linear detectors is still computationally expensive. Thus, the further exploration of this research in lowering the computational complexity of matrix inversion posed by linear data detection like MMSE data detection.

2.7.1 Formulation of the Uplink OTFS Massive MIMO Data Detection Model

With the channel estimation obtained, it is very important to have a good data detection technique that will help with obtaining the transmitted symbols. In OTFS massive MIMO, it is very difficult to detect the transmitted signals with an increase quantity of parameters and, faster channel statistics change.

Consider a u UE's with single transmit-receive antennas that transmit data to q receive antennas in a massive MIMO setup with frequency division duplex (FDD) based on OTFS modulation in [4]. The output signal at the receiver base station is represented by $\boldsymbol{y}$ in the system model in Figure 1.3.

For the *u*th UE antenna, the received signal in the delay-Doppler domain is

$$\boldsymbol{y}^u = \boldsymbol{H}^u \boldsymbol{d}^u + \boldsymbol{v}^u, \tag{2.27}$$

where H^u is the *u*th UE's delay-Doppler channel gain matrix, $\boldsymbol{v}^u$ represents the *u*th UE's AWGN occurred in the whole channel, and $\boldsymbol{d}^u$ represents the transmitted symbol vector of the *u*th UE information transmitted $\boldsymbol{a}$,

$$\boldsymbol{d}^u = \boldsymbol{V}^u \boldsymbol{a}^u, \tag{2.28}$$

where $\boldsymbol{V}$ is the precoding matrix. If data matrices of all UEs are stacked up to form a $Mu \times N$ matrix $\boldsymbol{B}$ as:

$$\boldsymbol{B} = \begin{bmatrix} \boldsymbol{D}^0 \\ \boldsymbol{D}^1 \\ \vdots \\ \boldsymbol{D}^{u-1} \end{bmatrix}, \tag{2.29}$$

where $\boldsymbol{D}^{u}$ is the 2D complex $M \times N$ data matrix of the uth UE. After *ISFFT* to each sub-matrix $\boldsymbol{D}^{u}$,

$$\boldsymbol{X} = (\boldsymbol{I}_q \otimes \boldsymbol{F}_M)\boldsymbol{B}{\boldsymbol{F}_N}^{H}. \tag{2.30}$$

$\boldsymbol{x}$ is the vectorized version of $\boldsymbol{B}$ according to Figure 1.3, defined as follows:

$$\boldsymbol{x} = \begin{bmatrix} b_0 \\ b_1 \\ \vdots \\ b_{N-1} \end{bmatrix}, \qquad \boldsymbol{b}_n = \begin{bmatrix} {\boldsymbol{b}_n}^{0} \\ {\boldsymbol{b}_n}^{1} \\ \vdots \\ {\boldsymbol{b}_n}^{u-1} \end{bmatrix}, \qquad {\boldsymbol{b}_n}^{j} = \begin{bmatrix} {\boldsymbol{b}_{0,n}}^{0} \\ {\boldsymbol{b}_{1,n}}^{1} \\ \vdots \\ {\boldsymbol{b}_{M-1,n}}^{u-1} \end{bmatrix}, \tag{2.31}$$

where ${\boldsymbol{b}_{m,n}}^{j}$ is the data symbol of the jth transmitting UE and $j = 0,1, \dots, u-1$. According to [4],

$$\bar{\boldsymbol{x}} = ({\boldsymbol{F}_N}^{H} \otimes \boldsymbol{I}_u \otimes \boldsymbol{F}_M)\boldsymbol{x}. \tag{2.32}$$

where $\bar{\boldsymbol{x}}$ is the vectorized version of $\boldsymbol{X}$. After partitioning $\bar{\boldsymbol{x}}$ to N blocks, $\bar{\boldsymbol{x}}_n$, the window function is multiplied by each block. If all UEs are considered to use the same window function by multiplying the vectorized data block $\bar{\boldsymbol{x}}$ by the transmitting windowing matrix $\bar{\boldsymbol{K}}_n$, $\boldsymbol{S}_n$ is obtained as follows:

$$\boldsymbol{S}_n = \bar{\boldsymbol{K}}_n \bar{\boldsymbol{x}}_n, \tag{2.33}$$

where $\bar{\boldsymbol{K}}_n = \boldsymbol{I}_u \otimes \boldsymbol{K}_n$, $\boldsymbol{K}_n$ is nth transmitting windowing function $\boldsymbol{w}^{tx}$. The Heisenberg transform in Figure 1.3, which is part of the OTFS modulation in Figure 1.2, will transform the frequency-time domain signal of each UE to the time-domain as:

$$\boldsymbol{s}_n = (\boldsymbol{I}_u \otimes \boldsymbol{F}_M{}^H)\boldsymbol{S}_n, \tag{2.34}$$

$$\boldsymbol{s} = (\boldsymbol{I}_{Nu} \otimes \boldsymbol{F}_M{}^H)\boldsymbol{S}. \tag{2.35}$$

The transmitter will add CP to the signal in the time domain to transmit and send through the channel. The receiver will first remove the CP, and after the received signal is CP free, as described below:

$$\begin{aligned} \boldsymbol{r}_n &= \left(\boldsymbol{I}_q \otimes \boldsymbol{R}_{CP}\right)\boldsymbol{H}_n(\boldsymbol{I}_u \otimes \boldsymbol{A}_{CP})\boldsymbol{s}_n + \boldsymbol{v}_n \\ &= \bar{\boldsymbol{H}}_n \boldsymbol{s}_n + \boldsymbol{v}_n, \end{aligned} \tag{2.36}$$

where $\boldsymbol{r}_n$ is the received signal in the time domain after removing the CP.

$$\bar{\boldsymbol{H}}_n = \begin{bmatrix} \bar{\boldsymbol{H}}_n{}^{0,0} & \bar{\boldsymbol{H}}_n{}^{0,1} & \cdots & \bar{\boldsymbol{H}}_n{}^{0,u-1} \\ \bar{\boldsymbol{H}}_n{}^{1,0} & \bar{\boldsymbol{H}}_n{}^{1,1} & \cdots & \bar{\boldsymbol{H}}_n{}^{1,u-1} \\ \vdots & \vdots & \ddots & \vdots \\ \bar{\boldsymbol{H}}_n{}^{q-1,0} & \bar{\boldsymbol{H}}_n{}^{q-1,1} & \cdots & \bar{\boldsymbol{H}}_n{}^{q-1,u-1} \end{bmatrix}. \tag{2.37}$$

$\bar{\boldsymbol{H}}_n{}^{r,j}$ is the *n*th CIR matrix between *j*th UE and *q*th receive antenna. As a result, according to Figure 1.3,

$$\boldsymbol{r} = \bar{\boldsymbol{H}}\boldsymbol{s} + \boldsymbol{v}, \tag{2.38}$$

where $\bar{H}$ is $diag\{\bar{H}_n\}$. The output of the Wigner Transform, according to Figure 1.3 will be:

$$\bar{\boldsymbol{r}} = (\boldsymbol{I}_{Nq} \otimes \boldsymbol{F}_M)\boldsymbol{r}. \tag{2.39}$$

$\bar{\boldsymbol{r}}$ is the length MNq frequency-time signal vector. Lastly, after the signal is multiplied by the receiving windowing function, it gets mapped with the delay-Doppler domain and finally, the estimation of the transmitted signal can be obtained as:

$$\boldsymbol{y} = (\boldsymbol{F}_N \otimes \boldsymbol{I}_q \otimes \boldsymbol{F}_M{}^H)\boldsymbol{Y}, \tag{2.40}$$

where $\boldsymbol{Y}_m = \bar{\boldsymbol{P}}_m \boldsymbol{R}_m$, $\bar{\boldsymbol{P}}_m = \boldsymbol{I}_q \otimes \boldsymbol{P}_m$, $\boldsymbol{P}_m$ is the mth receiving windowing function. Using equations from (2.27) to (2.40), it is easier to formulate a relationship to obtain the estimation of the channel and the transmitted signal. However, most CE techniques in the literature are difficult to implement directly for OTFS massive MIMO systems because of the massive number of antennas, as detailed in [22]. The massive number of antennas is directly proportional to the number of transmitting orthogonal pilots, which leads to high pilot overhead and high pilot contamination in a multi-cell multi-user system. The OTFS massive MIMO system in equations (2.27) to (2.40) implements impulses in the delay-Doppler domain as pilots. Every UE transmitting and base station antenna receiving pair has a unique channel. The delay-Doppler spread of the CIR determines finite support in each channel as in [22]. As a result, the channel statistic of each transmit UE and receive base station antenna equipment pairs simultaneously using one OTFS massive MIMO frame can be obtained. The OTFS transceiver relationship for uth transmit UE, and qth receive antenna can be illustrated as:

$$\boldsymbol{y_q}[k,l] = \sum_{m=0}^{M-1} \sum_{n=0}^{N-1} \boldsymbol{x}_u[n,m] \frac{1}{MN} \boldsymbol{H}_{uq}\left(\frac{k-n}{NT} - \frac{l-m}{M\Delta f}\right) + \boldsymbol{v_q}[k,l], \tag{2.41}$$

where $l = 0, \ldots, M\text{-}1$ and $k = 0, \ldots, N\text{-}1$.

2.8 Chapter Summary

This chapter presents an overview of the channel models for OTFS, massive MIMO, and OTFS massive MIMO systems. An informed description of OTFS, massive MIMO, and OTFS massive MIMO systems have been provided in this chapter to help shed light on how the systems operate. Merits of the channel models for OTFS, massive MIMO, and OTFS massive MIMO systems are stipulated. According to the literature presented in this chapter, there is a great need for efficient CE and data detection for OTFS massive MIMO in wireless systems. From the literature highlighted in this chapter, some improvements need to be made in channel estimation to improve pilot-overhead, great convergence rate, and good performance. Moreover, efficient data detection is highlighted in this chapter to improve the computational complexity of the OTFS massive MIMO system. To formulate efficient CE and data detection, good OTFS massive MIMO models are required. As a result, downlink and uplink OTFS massive MIMO models are presented in this chapter.

Chapter 3 - CoSaMP Channel Estimation with interleaving for Downlink OTFS Massive MIMO

3.1 Introduction

In this chapter, downlink channel estimation is formulated as a sparse recovery problem. The channel estimation problem is viewed as the multiple measurement vector problem in compressive sensing theory. The channel estimation technique proposed in this part of the research improves pilot overhead performance and error performance in high-Doppler scenarios, which are prominent problems in downlink OTFS massive MIMO systems. The implementation of the traditional Compressive Sampling Matching Pursuit (CoSaMP) in delay-Doppler scenarios but with additional interleaving to better the error performance of the OTFS massive MIMO system is developed. Subsequently, the performance evaluation of the proposed channel estimation is presented and discussed. The simulation results graphically show that the proposed technique has some valuable merits, and it closes some gaps in the literature.

3.2 The Proposed CoSaMP channel estimation with interleaving

Consider a single cell with a base station transmitting signals to a single antenna user equipment as described in Figure 1.4. The base station has a uniform linear array (ULA), which contains q antenna elements. The mobility of the user equipment makes the channel vary with respect to time, i.e., the channel links experience time selective fading. The OTFS massive MIMO system in consideration implements impulses in the delay-Doppler domain as pilots. Every individual UE that transmits information and every base station antenna that receives information has a unique channel and the delay-Doppler spread of the CIR determines finite support in each channel [22] and as a result, the channel statistic of each transmit antenna and receive user-equipment pairs simultaneously using one OTFS massive MIMO frame can be obtained. The OTFS transmit-receive relation for qth transmit antenna, and uth receive user equipment can be illustrated as:

$$\boldsymbol{y}[k,l] = \sum_{m=0}^{M-1}\sum_{n=0}^{N-1} \boldsymbol{x}_q[n,m]\,\frac{1}{MN}\boldsymbol{H}_q\left(\frac{k-n}{NT} - \frac{l-m}{M\Delta f}\right) + \boldsymbol{v}[k,l], \tag{3.1}$$

where l = 0, …, M-1 and k = 0, …, N-1. Consider the length of pilot symbols along the delay and Doppler dimensions to be M_τ and N_v, respectively. As a result of the delay-Doppler channel $\bar{\boldsymbol{H}}$ in OTFS massive MIMO systems having finite supports along the delay and Doppler dimensions, the guard intervals (G_N for Doppler) and (G_M for the delay) should have a length greater than or equal to delay finite supports and Doppler finite supports, i.e., $G_M \geq M_{max} - 1$ along delay dimension and $G_N \geq N_{max}$. The mobility of the UE causes the channel links to experience time-selective fading. The OTFS massive MIMO system in consideration implements pilot symbols in the delay-Doppler domain to obtain the effects of the channel on the transmitted signal. The transmit pilot symbols at different antennas completely overlap each other in the delay-Doppler domain. As a result, non-orthogonal complex Gaussian random pilots in the delay-Doppler domain at the transmit antennas are considered to reduce pilot overhead because random pilot symbols at different transmit antennas are independent. The non-orthogonal complex Gaussian random pilot symbols in the delay-Doppler domain at the (q+1)-th transmit antenna are considered and denoted as $x_q[k,l]$ ($k = 0,1,\dots,M_\tau - 1,\ l = \frac{-N_v}{2},\dots,0,\dots,\frac{N_v}{2} - 1$). The OTFS frames at the qth transmit antennas are modulated and transmitted simultaneously. After passing the channel, the received signal is demodulated, and the guard intervals are removed. Transmit antenna q's received pilots in the delay-Doppler domain at the user-equipment can be expressed as:

$$\boldsymbol{y}[k,l] = \sum_{p=1}^{P} \boldsymbol{b}[k-m,n]\boldsymbol{H}_q[m,n]\boldsymbol{x}_q[k-m,l-n] + \boldsymbol{v}[k,l], \tag{3.2}$$

where $\boldsymbol{b}[k-m,n] = e^{j2\pi\frac{(k-m)n}{N(M+N_{CP})}}$ is the compensate phase, $m = 0,1,\dots,G_M$ and $n = \frac{-G_N}{2},\dots,0,\dots,\frac{G_N}{2}$. As a result of simplification in [17], (3.2) can be further simplified as:

$$\boldsymbol{y} = \boldsymbol{b} \odot \boldsymbol{x}_q \boldsymbol{h}_q + \boldsymbol{v}. \tag{3.3}$$

The proposed CoSaMP-based channel estimation technique views every delay-Doppler constellation symbol $\boldsymbol{x}$ as mutually independent, and several subsequent delay-Doppler symbols are considered a transmission group. Hence, the structured nature of the transmitted

symbols allows more reliable channel estimation and improves the error performance of the system. Due to the quasi-static nature of the delay-Doppler channels in OTFS massive MIMO systems in consecutive transmission groups of symbols, the channels get into deep fading, which weakens the channel estimation of the system. Interleaving is further introduced at the transmitter to alleviate the problem of deep fading [69]. Interleaving in the same transmission group is different in different delay-Doppler spaces and is known by both transmitter and receiver. Hence, transmission antennas vary in different delay-Doppler spaces from the same transmission. Thus, channel diversity can be appropriately exploited to better the channel estimation process at the receiver.

By considering CoSaMP-based channel estimation with interleaving at the receiver in the same delay-Doppler space, equation (3.3) can be formulated as

$$\boldsymbol{y}^{d} = \boldsymbol{b}\odot\boldsymbol{\Pi}^{d}\boldsymbol{x}^{\boldsymbol{d}}{}_{q}\boldsymbol{h}^{d}{}_{q} + \boldsymbol{v}^{d}, \tag{3.4}$$

where $\boldsymbol{b}\odot\boldsymbol{\Pi}^{d}\boldsymbol{x}^{\boldsymbol{d}}{}_{q}$ is the deinterleaving process and the sparse sensing matrix and $d(1,2,..,D)$ are the number of common multiple measurement support sets that those multiple sparse signals share. From (3.4), the delay-Doppler channel is sparse but with different nonzero areas [69]. With that in mind, CS techniques can be used to estimate the delay-Doppler channel of the system.

3.2.1 Summary of the Proposed CoSaMP-based channel estimation with interleaving

The proposed CoSaMP algorithm with interleaving is described in Algorithm 3.1. Step 1 to step 5 of the algorithm performs the input and initialization of the parameters in the algorithm. Step 8 and step 9 obtain the proper dominant delay-Doppler supports of each dominant path and merge the current supports with the previous supports of the prior iteration. Steps 10 - 12 aim at updating the delay-Doppler supports by eliminating the wrong delay-Doppler supports. Finally, the residual value is updated, the stopping criterion is checked, and if met, the channel estimation value is obtained.

Algorithm 3.1: Proposed CoSaMP-based channel estimation with interleaving

1. ***Input:*** Observation vector $\boldsymbol{y}$
   Sensing matrix $\boldsymbol{\psi} = (\boldsymbol{b} \odot \boldsymbol{\Pi}^{\boldsymbol{d}} \boldsymbol{x}^{\boldsymbol{d}}{}_{\boldsymbol{q}})$
   Active BS antennas $\boldsymbol{q}^{\boldsymbol{ac}}$
   Iteration $\boldsymbol{K}$
   Maximum iteration
2. ***Initialization***
3. ϕ=∅
4. Residual value $\boldsymbol{y_r} = \boldsymbol{y}$
5. $\boldsymbol{iter}$ =**0**
6. ***Iteration***
7. Increase number of iterations $\boldsymbol{iter} = \boldsymbol{iter} + \mathbf{1}$
8. $\boldsymbol{p_{iter}} = \{\boldsymbol{c} | \boldsymbol{c} = \boldsymbol{y_{r_{iter}}}, \boldsymbol{\psi}\}$
9. $\boldsymbol{\gamma} = \boldsymbol{\phi_{iter-1}} \cup \boldsymbol{p_{iter}}$
10. $\boldsymbol{s} = \boldsymbol{\psi_{\gamma}}^{\dagger} \boldsymbol{y}$
11. $\boldsymbol{\phi_{iter}} = \{\boldsymbol{c} | \boldsymbol{c} = \boldsymbol{y_{r_{iter}}}, \boldsymbol{s}\}$
12. $\boldsymbol{e_{\phi_{iter}}} = \boldsymbol{\psi_{\phi_{iter}}}^{\dagger} \boldsymbol{y}$
13. $\boldsymbol{y_r} = \boldsymbol{y} - \boldsymbol{\psi' e}$
14. ***(Termination condition)***
15. If $\boldsymbol{iter} \geq \boldsymbol{maximum\ iteration\ or} \left\|\boldsymbol{y_{r_{iter}}}\right\|_2 > \left\|\boldsymbol{y_{r_{iter-1}}}\right\|_2$, quit iteration
16. $\check{\boldsymbol{h}}_{\boldsymbol{iter}} = \boldsymbol{e}$
17. ***Output:*** $\check{\boldsymbol{h}}$

3.3 Performance of the CoSaMP-based CE with signal interleaving

The merit of the performance of the proposed channel estimation technique with interleaving is discussed by comparing the CoSaMP channel estimation probability with and without interleaving. By assuming that the sensing matrix $\boldsymbol{\psi}$ for any given BS antenna in a group of delay-Doppler symbols are mutually independent, the received signal can be formulated as

$$\boldsymbol{y}^{d} = \boldsymbol{\psi}^{d} \check{\boldsymbol{h}}^{d} + \boldsymbol{v}^{d}, \tag{3.5}$$

where $\check{\boldsymbol{h}}$ is the channel statistic in a group of delay-Doppler symbols. The proposed CoSaMP algorithm relies on the correlation operation in step 8 to identify the channel estimation of each antenna path.

$$\begin{aligned} P_b &= \sum_{1}^{d} |y_d{}' \psi_d|^2 \\ &= \textstyle\sum_1^d \left|(\varphi_d \psi^a{}_d + v_d)' \psi^a{}_d\right|^2, \end{aligned} \tag{3.6}$$

where $(\varphi_d {\psi^a}_d + v_d)' {\psi^a}_d$ can be substituted by ${\alpha^{a,b}}_d$ for $1 \leq a, b \leq q$. Due to the massive number of antennas, according to the central limit theorem in [69], there is $\text{Re}\{{\alpha^{a,a}}_d\} \sim \mathcal{N}(\mu_1, {\sigma^2}_1)$ with $\mu_1 = 0$, ${\sigma^2}_1 = (\frac{(q^2+q){\sigma_s}^2}{2-\delta(A=2)} + (q{\sigma_v}^2/2)$, and $\text{Im}\{{\alpha^{a,a}}_d\} \sim \mathcal{N}(\mu_2, {\sigma^2}_2)$ with $\mu_2 = 0$, ${\sigma^2}_2 = \left(\left(1 - \delta(A=2)\right)(q^2+q){\sigma_s}^2\right) + (q{\sigma_v}^2/2)$. It is important to note that ${\sigma_s}^2 = Tr\left\{E\left\{h_d {h_d}^T\right\}\right\}$ and $\text{Re}\{{\alpha^{a,b}}_d\}$ and $\text{Im}\{{\alpha^{a,b}}_d\}$ are mutually independent for all values of b [69]. Algorithm 3.1 has one iteration for which the active antenna $q^{ac} = 1$. As a result, the generalized multiple measurement vector probability has $(P_a - {P_b}^{[2]} > 0 | a \neq b)$ as the antenna channel estimation probability where ${P_b}^{[1]} > {P_b}^{[2]} > \cdots > {P_b}^{[q-q^{ac}]}$ with $a \neq b$ sequential statistics. The pdf of P_a and P_b where $a \neq b$ are denoted by $g_1(x)$ and $g_2(x)$, respectively. According to [69], the pdf of ${P_b}^{[2]}$ with $a \neq b$ is $g_2(x) = (q - q^{ac})!/(q - q^{ac} - 2)!\,(G_2(x))^{q-q^{ac}-2}(1 - G_2(x))g_2(x)$, where $G_2(x)$ is the cumulative density function of $g_2(x)$. Thus, having the correct antenna channel estimation probability as

$$P_a - {P_b}^{[2]} > 0 | a \neq b = \int_0^\infty \int_{-\infty}^\infty g(x) {g^{[2]}}_2(x - z)\, dx dz. \tag{3.7}$$

By comparing the correct antenna channel estimation probability for multiple measurement vector and generalized multiple measurement vector when d is large, we can see that $P_a - P_b$ can be approximated to Gaussian distribution $\mathcal{N}(\mu_4, {\sigma^2}_4)$ with $\mu_4 = d({\mu_1}^2 + {\mu_2}^2 - 2{\mu_3}^2 + {\delta_1}^2 + {\sigma_2}^2 - 2{\sigma_3}^2)$, ${\sigma_4}^2 = d\sum_{j=1}^3 2{\sigma_j}^4 + 4{\mu_j}^2{\sigma_j}^2$. In this way, it is discovered that the correct antenna channel estimation probability of generalized multiple measurement vector is approximately equal to $I(-\mu_4/\sigma_4)$, where I-function is the tail probability of the standard normal distribution [69]. On the other hand, the correct antenna channel estimation probability of the conventional multiple measurement vector is approximately equal to $I(-\mu_4/\sqrt{d}\sigma_4)$ [69]. As a result, it is very clear that the correct antenna channel estimation problem for the multiple measurement vector is greater than the correct antenna channel estimation probability for the generalized multiple measurement vector which shows that interleaving will improve channel estimation for OTFS massive MIMO.

3.4 Computational Complexity Performance

The computational complexity cost of the CS estimator in massive MIMO relies on the sparsity level, the number of BS antennas and the number of users in the considered system [23]. In case of sparse signals with $K \leq const.\sqrt{N_{max}}$, which is the case in certain scenarios in communication systems, the computational complexity of a system with q antennas is upper bounded by $\mathcal{O}(KN_{max}M_{max}q)$.Since the 3D-SOMP algorithm runs through K iterations, the reconstruction computational complexity is roughly $\mathcal{O}(KN_{max}M_{max}q)$. According to [23], since CoSaMP without interleaving does rely on sparsity level and it runs through $2K$ iterations, the computational complexity is $\mathcal{O}(2N_{max}M_{max}qK)$, and for the proposed CoSaMP with interleaving, the algorithm runs through $2K$, considers active antennas, and the non-zero entries of the sparse signal decay slowly, the computational complexity can be reduced to $\mathcal{O}((q+q^{ac})N_{max}M_{max}\log 2K)$. The proposed CoSaMP-based estimator with interleaving has a better computational complexity cost than the ordinary CoSaMP-based estimator. This is mainly because the sparse signal of the proposed CoSaMP-based estimator with interleaving's non-zero entries decays slowly, which makes it have better performance and low pilot overhead requirements, making it more bandwidth-efficient.

Table 3.1: Computational complexity values for a scenario in OTFS massive MIMO

Channel Estimator	**Computational Complexity**	**Numerical Values** (**q=64, $q^{ac}=2$, M_{max}=600, N_{max}=12, K=6**)
CoSaMP-based estimator without interleaving	$\mathcal{O}(2N_{max}M_{max}qK)$	≈ 5 529 600
3D-SOMP-based estimator	$\mathcal{O}(KqN_{max}M_{max})$	≈2 764 800

Proposed CoSaMP-based estimator with interleaving	$\mathcal{O}((q+q^{ac})N_{max}M_{max}log2K)$	≈512 826

3.5 Simulation Results

This section presents the performance evaluation of the proposed CoSaMP-based channel estimation technique by interleaving in a single transmitting urban macro-cell with one single antenna receiving user equipment to lower computational simulation complexity. The system used in the simulation to evaluate the proposed CoSaMP-based estimator has a carrier frequency of 2.15 GHz and is operating in FDD. In this work, there is an evaluation of the 15kHz sub-carrier spacing of the system, and the cyclic prefix rate used to alleviate inter-symbol interference is 16.6 micro-seconds [1],[18]. The simulations explore the OTFS scheme, which operates efficiently and effectively in high-Doppler scenarios that can get to 500km/h or more [24]. As the system is supposed to provide dynamic performance in both low and high-Doppler scenarios, the performance evaluations include speeds from 72km/h to 576km/h, which are the envisaged speeds in wireless communications systems in both 5G and beyond 5G networks. According to [70], a traditional MIMO system has up to 8 antenna elements, and a massive MIMO system has at least 16 antenna elements. However, massive MIMO enables highly efficient and effective transmissions in systems with at least 64 antennas [71]. As a result, the performance evaluation in this section considers systems with 64 BS antenna elements to articulate the performance of the proposed estimator in a massive MIMO system. In all the simulations, it is assumed that there is perfect synchronization between UEs and the BS.

For the performance index, mean square error, normalized by the signal power of the system referred to as NMSE, is employed and expressed as follows:

$$NMSE = \frac{\|\hat{\boldsymbol{H}}-\boldsymbol{H}\|^2}{\|\boldsymbol{H}\|^2}, \tag{3.8}$$

where the estimated channel is $\widehat{\boldsymbol{H}}$ and $\boldsymbol{H}$ is the right channel of the system. Due to high-Doppler scenarios in the OTFS modulation scheme and a massive number of antennas in a massive MIMO system, addressing the pilot overhead ratio is still a big problem in this research. As a result, this section compares pilot overhead ratios of the traditional impulse response channel estimation scheme, the 3D-SOMP-based estimator [17], and the CoSaMP-based scheme.

Figure 3.1 shows the simulation results of the performance of the proposed CoSaMP-based estimator with interleaving against CoSaMP-based estimator without interleaving and the 3D-SOMP-based estimator in [17].

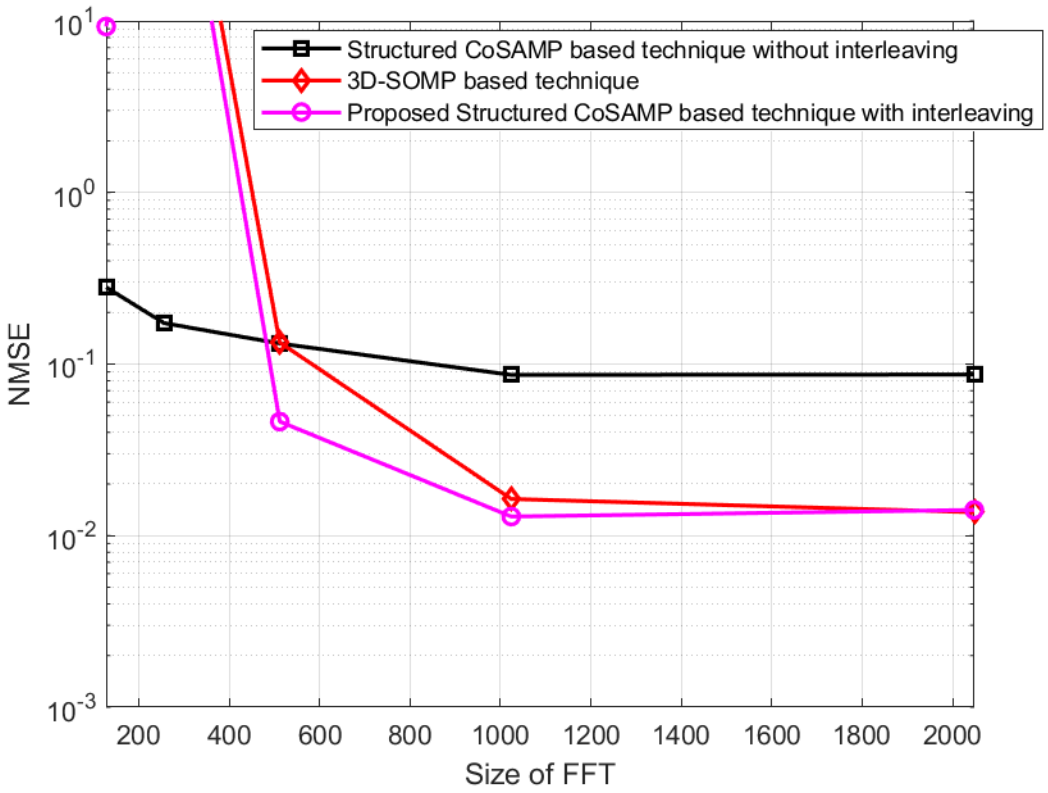

Figure 3.1: NMSE vs Size of FFT for CoSaMP-based channel estimation without interleaving, 3D-SOMP channel estimation technique, and proposed CoSaMP-based channel estimation with interleaving

Different FFT sizes were considered to investigate how the proposed channel estimation method affects the resolution of the resulting spectra. According to Figure 3.1, the proposed CoSaMP with interleaving has better performance in a lower spectral resolution under high-Doppler scenarios in OTFS massive MIMO. The better performance is mainly because the consistent updating of the support paths in the algorithm helps the algorithm fight through the

setbacks of traditional sampling, significantly lowers sampling frequency and improve the transmission burden introduced by high-Doppler scenarios.

In Figure 3.2, the proposed CoSaMP-based channel estimator graphically proves better pilot overhead performance in high-Doppler scenarios.

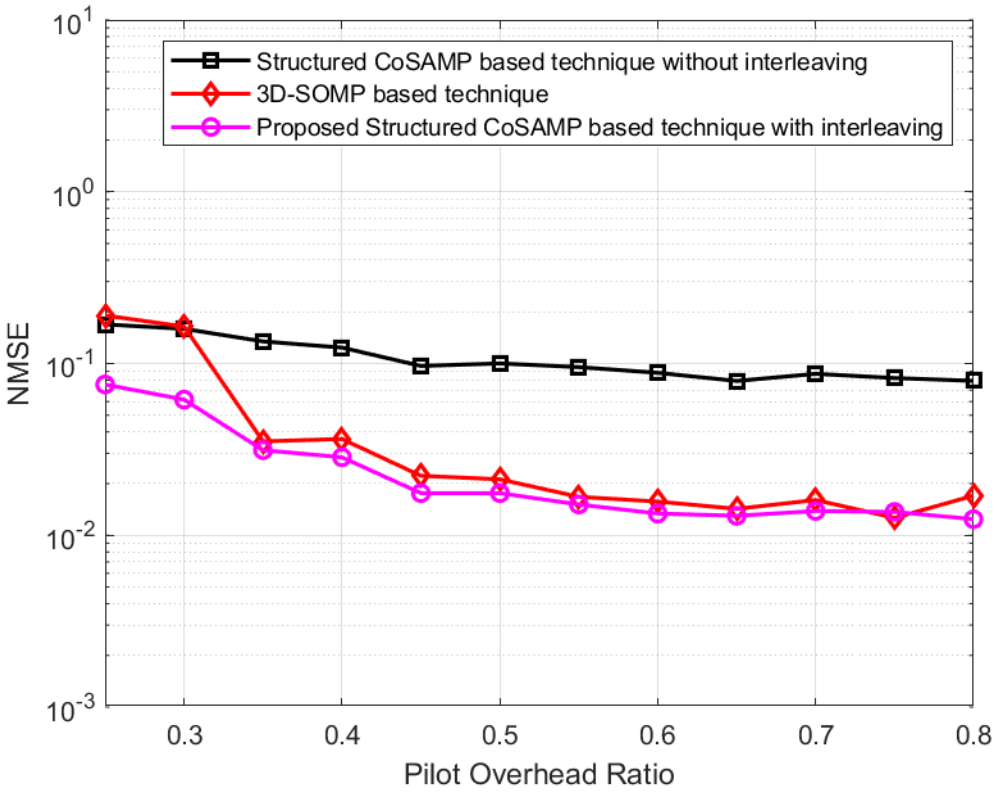

Figure 3.2: NMSE vs Pilot Overhead Ratio for CoSaMP-based channel estimation without interleaving, 3D-SOMP channel estimation technique, and proposed CoSaMP-based channel estimation with interleaving

The proposed channel estimation technique improves the issue of pilot overhead in downlink OTFS massive MIMO. The performance improvement is mainly because the backtracking nature of the technique lowers the probability of error accumulation. The possibility of error accumulation is a shortcoming in 3D-SOMP as the atoms cannot be altered once deposited in the candidate set, requiring more pilot symbols for channel estimation due to the errors [72]. As a result, the proposed CoSaMP-based channel estimation technique with interleaving demonstrates improved channel estimation accuracy and robustness, desirable traits in high-

Doppler scenarios. As a result, the proposed channel estimator exhibits better performance at low pilot overhead. The proposed channel estimator improves bandwidth efficiency of the OTFS massive MIMO system.

The ability of the proposed CoSaMP-based channel estimator with interleaving to perform well with low pilot overhead makes it a great candidate in OTFS massive MIMO systems. The simulation results in Figure 3.3 show that the proposed estimator exhibits better performance in higher SNR values.

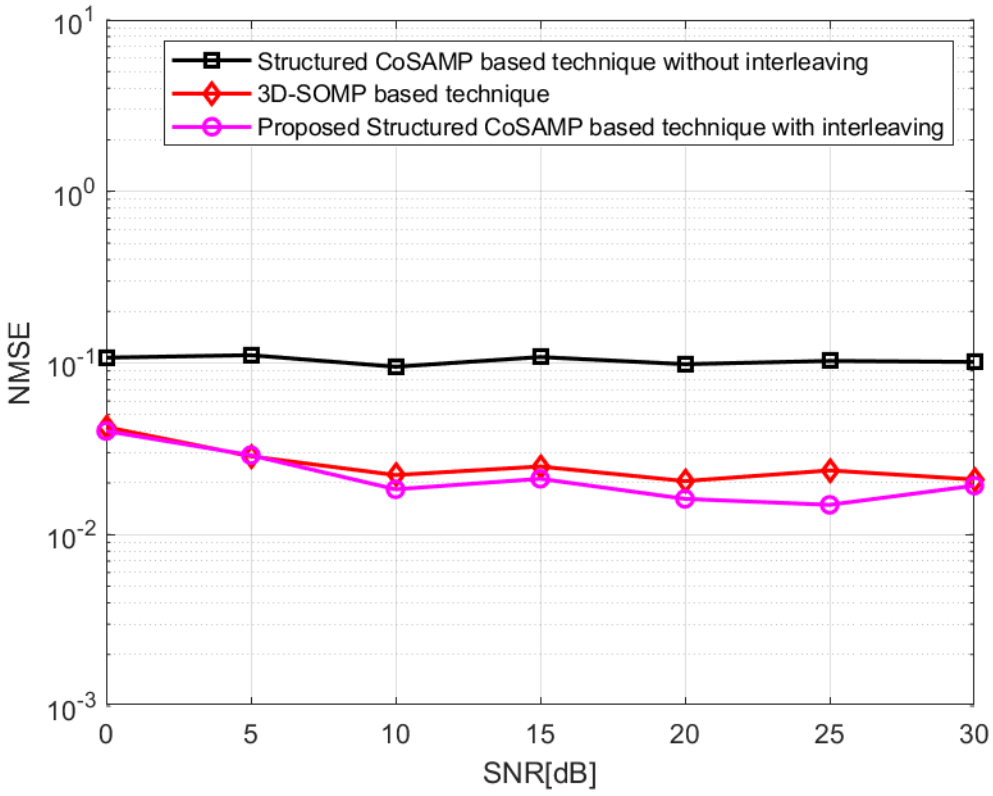

Figure 3.3: NMSE vs SNR for CoSaMP-based channel estimation without interleaving, 3D-SOMP channel estimation technique, and proposed CoSaMP-based channel estimation with interleaving

This is because the constant updating of the support sets improves the reconstruction process of the signals containing much noise in high-Doppler scenarios compared to the 3D-SOMP-based estimator [73]. As much as the CoSaMP-based channel estimator without interleaving

has potential in high-Doppler scenarios, it still lacks stability in high-Doppler scenarios and systems with many antennas [74], which makes it possible exhibit poor performance.

Figure 3.4 shows that the proposed CoSaMP-based channel estimator performs better in lower velocities and higher velocities.

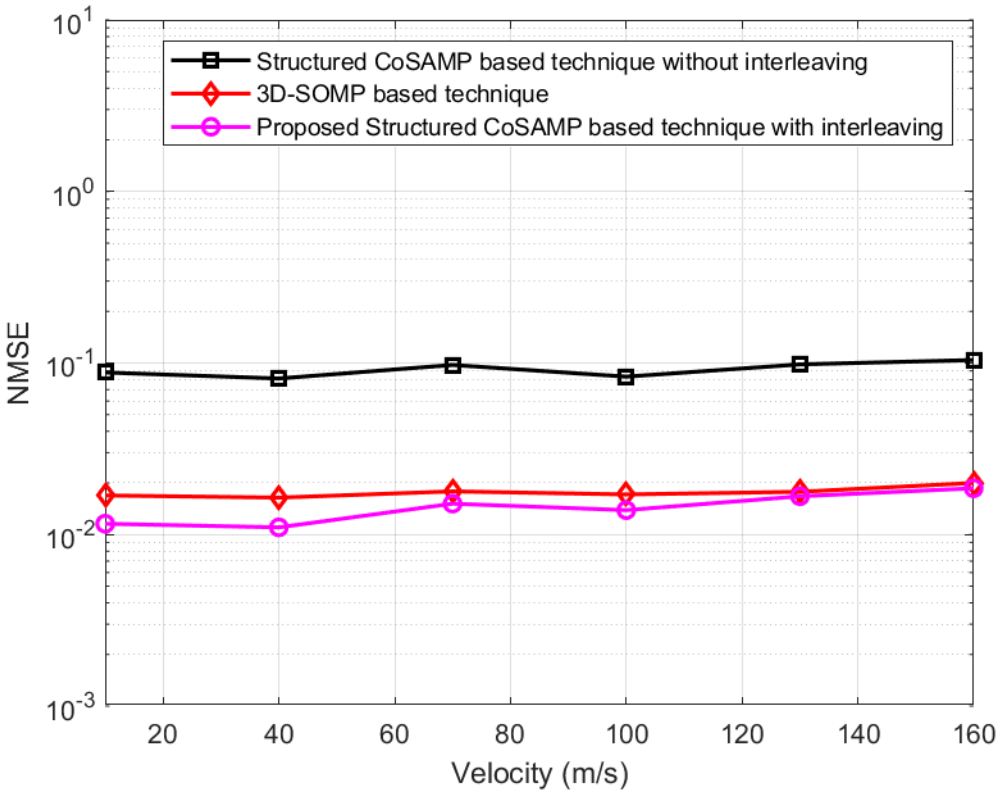

Figure 3.4: NMSE vs Velocity for CoSaMP-based channel estimation without interleaving, 3D-SOMP channel estimation technique, and proposed CoSaMP-based channel estimation with interleaving

The stability of the proposed channel estimation technique introduced by interleaving, good performance in low pilot overhead, and consistent updating of the channel estimation support sets makes the proposed channel estimator have better performance. The high velocities expected in OTFS massive MIMO systems make the channel estimation process require more pilot symbols for accurate channel estimation. However, the backtracking ability in the proposed estimator improves the system's channel estimation and reconstruction process and, hence, the better performance in high-Doppler scenarios.

3.6 Chapter Summary

This chapter proposed a CoSaMP-based channel estimation technique with interleaving for OTFS massive MIMO systems. The delay-Doppler channel in the OTFS massive MIMO system is viewed as a multiple measurement vector problem due to the correlation of subsequent delay-Doppler symbols transmitted in the system. As a result, the downlink channel estimation problem as a multiple sparse signal recovery problem is formulated and solved using the proposed CoSaMP-based channel estimation scheme with interleaving. Simulations are performed based on the system model presented in this chapter. Simulation results prove that the proposed estimator has better performance in the OTFS massive MIMO systems than the other estimators. The proposed CoSaMP-based estimator with interleaving incurred better performance at low pilot overhead, proving bandwidth efficiency. Hence, the proposed estimator is a good candidate for OTFS massive MIMO-based 5G and beyond 5G wireless communication in terms of performance.

Chapter 4 - Delay-Doppler Subspace Pursuit-based Channel Estimation for Downlink OTFS Massive MIMO System

4.1 Introduction

In this chapter, downlink channel estimation is formulated as a sparse recovery problem in OTFS massive MIMO system. In chapter 2, different channel estimation techniques were explored and formulated for the downlink OTFS massive MIMO system model. With the pilot overhead ratio and computational complexity proportional to the number of antennas, this chapter presents a compressive sensing-based channel estimation technique that lowers the pilot overhead ratio, lowers computational complexity, and improves the error performance of downlink OTFS massive MIMO systems. However, the main difference between the proposed channel estimator in this chapter and the channel estimator in chapter 3 is that the proposed channel estimator only adds P candidates to the support sets. In contrast, the channel estimator in chapter 3 adds $2P$ candidates which makes the proposed channel estimator in this chapter computationally more efficient. As a result, the proposed channel estimator requires less number of iterations to reach its optimal performance. There is an articulation of the detailed knowledge about the system model adopted for this proposed channel estimation technique. In the proposed CE scheme, a single user rather than a multi-user scenario is assumed for simplicity and to help focus and address the efficiency issues of the proposed channel estimation technique to close the identified gaps in the literature. The proposed CE scheme, the Delay-Doppler Subspace Pursuit (DDSP)-based CE scheme from the traditional Subspace Pursuit algorithm and implemented for the OTFS massive MIMO system. After that, computer simulations are executed to articulate the comparative performances of the proposed channel estimation method. The obtainable simulation results show that the proposed CE technique has exhibited admirable merits that make it stand out for employment in OTFS massive MIMO wireless communication systems.

4.2 Derivation of the Proposed DDSP-based Algorithm

Consider a single cell with a base station transmitting signals to a single antenna user equipment as described in Figure 1.4. The base station has a ULA, which contains q antenna elements. Downlink OTFS massive MIMO can be further simplified as:

$$\boldsymbol{y} = \boldsymbol{b} \odot \boldsymbol{x}_q \boldsymbol{h}_q + \boldsymbol{v}. \tag{4.1}$$

If $\boldsymbol{b} \odot \boldsymbol{x}_q$ is considered as the sensing matrix $\boldsymbol{\beta}$, (4.1) can be further simplified to produce:

$$\boldsymbol{y} = \boldsymbol{\beta} \boldsymbol{h}_q + \boldsymbol{v}. \tag{4.2}$$

Implementation of compressive sensing algorithms can solve the problem in (4.2). There must be an expression of initialization of the model in Figure 1.4 as a sparse signal in the delay-Doppler domain. It can be easier to find out the subspace in which the received signal lies to implement the DDSP-based technique. The estimator then determines the nonzero signal coefficients by continuously refining the estimate by keeping the reliable candidates and eliminating of the unreliable ones while adding the same number of new candidates. As a result, the estimator can get the updated delay-Doppler candidate for channel estimation of the OTFS massive MIMO system.

There is a derivation of the proposed DDSP-based estimator from the main idea of the subspace algorithm. Selection of the right sparsity level for the DDSP-based estimator for OTFS massive MIMO system is crucial as it improves the algorithm's efficiency in high-Doppler scenarios. The proposed DDSP-based estimator aims to find delay-Doppler supports for each dominant path. The initial delay-Doppler supports are found by getting the top K^1 (where 1 represents the index of the supports) supports in the product of $\boldsymbol{\beta}'$ and $\boldsymbol{y}$.

$$\boldsymbol{c}_1 = \boldsymbol{\beta}' * \boldsymbol{y}. \tag{4.3}$$

The delay-Doppler supports indices K of the first dominant path is found by getting the largest element of $\boldsymbol{c}_1$. After obtaining the initial delay-Doppler supports of the first dominant path, the user equipment gets the residual value of the first dominant path.

$$\boldsymbol{y}_r{}^1 = \boldsymbol{y} - (\boldsymbol{\beta}(:, K^1) \times \boldsymbol{\beta}^{-1}(:, K^1) \times \boldsymbol{y}). \tag{4.4}$$

The next steps will be the iterations to find the updated support sets K^p of p dominant paths at random and generate the sparse channel statistic vector $\widetilde{\boldsymbol{h}}$ by selecting elements of the channel statistic vector $\widetilde{\boldsymbol{h}}$ restricted to K, that is,

$$\widetilde{\boldsymbol{h}} = \boldsymbol{\beta}^{-1}(:, K^p) \times \boldsymbol{y}. \tag{4.5}$$

Finally, the residual value and $\widehat{\boldsymbol{h}}$ the estimate of $\widetilde{\boldsymbol{h}}$ are obtained. $\widehat{\boldsymbol{h}}$ is then compared to $\widetilde{\boldsymbol{h}}$ to find the most optimum value of the channel statistic estimate. The proposed DDSP-based estimator for OTFS massive MIMO system is summarized in Algorithm 4.1.

Algorithm 4.1: Proposed DDSP-based channel estimator

1. ***Input:*** Observation vector $\boldsymbol{y}$
   Sensing matrix $\boldsymbol{\beta} \boldsymbol{\epsilon} \mathbb{R}^{\boldsymbol{m} \times \boldsymbol{N}}$
   Select the right sparsity level value $(\boldsymbol{K} \ll \frac{\boldsymbol{m}}{\boldsymbol{2}})$
2. ***Initialization:*** $\boldsymbol{p = 0}$
   $\boldsymbol{DD^0}$ = {$\boldsymbol{K}$ indices which correspond to the maximum delay-Doppler magnitude entries in $\boldsymbol{\beta}$ and $\boldsymbol{y}$}
   Find residual value $\boldsymbol{y_r{}^0}$ basing on $\boldsymbol{\beta_{DD^0}}$ and $\boldsymbol{y}$
3. **for** $\boldsymbol{p \leq P}$ **do**
4. $\boldsymbol{p = p + 1}$
5. $\widetilde{\boldsymbol{DD}}^{\boldsymbol{p}} = \boldsymbol{DD^s} \cup \{\boldsymbol{K}$ indices which correspond to the maximum delay-Doppler magnitude entries in $\boldsymbol{\beta}$ and $\boldsymbol{y_r{}^{p-1}}\}$
6. Set initial channel statistic estimate $\widetilde{\boldsymbol{h}}$ according to $\boldsymbol{\beta_{DD^p}}$ and $\boldsymbol{y}$
7. $\boldsymbol{DD^p}$ = {$\boldsymbol{K}$ indices which correspond to the maximum delay-Doppler magnitude entries in $\widetilde{\boldsymbol{h}}$}
8. Find the residual value $\boldsymbol{y_r{}^p}$ basing on $\boldsymbol{\beta_{DD^p}}$ and $\boldsymbol{y}$
9. **if** $\|\boldsymbol{y_r{}^p}\|_2 > \left\|\boldsymbol{y_r{}^{p-1}}\right\|_2$, {quit iteration}
10. ***Output:*** The estimated channel statistic $\widehat{\boldsymbol{h}}_{\boldsymbol{DD^p}}$ basing on $\boldsymbol{\beta_{DD^p}}$ and $\boldsymbol{y}$

4.3 Computational Complexity and Pilot Overhead Comparison

According to [17], pilot overhead is the length of measurement signals (training symbols), i.e., the ratio of training symbols transmitted against data symbols transmitted. The lower the pilot overhead, the higher the number of data symbols transmitted. The traditional impulse-based

estimator in an OTFS massive MIMO system has a pilot overhead of approximately $qN_{max}M_{max}$ [17]. According to [17] and [75], the compressive sensing theory states that pilot overhead is influenced by the sparsity level (L) and length of the sparse channel (θ). As a result, pilot overhead in compressive sensing channel estimators is approximately equal to $L\log\theta$. The 3D-SOMP-based estimator has a pilot overhead of approximately $N_{max}PD\log G_N G_M q$, where P is the number of iterations and D is the angle domain length. The proposed DDSP-based estimator has the pilot overhead of approximately $N_{max}P\log G_N G_M q$, which is why the DDSP-based estimator has superior pilot overhead performance. This is mainly due to the 3D-structured sparsity nature of the 3D-SOMP-based estimator, which makes it require a little bit more pilot symbols for exact recovery signal in high-Doppler scenarios, which makes it exhibit a worse NMSE performance with the low pilot overhead ratio as compared to the DDSP-based estimator in higher Doppler scenarios [17]. Additionally, the computational complexity of a compressing sensing estimator in massive MIMO depends on the number of iterations, the total number of base station antennas, and the total number of users for the complete reconstruction of the transmitted signal [23], [76]. The computational complexity of the traditional impulse-based estimator is approximately $\mathcal{O}(M_{max}q^2)$ and for the 3D-SOMP-based estimator is approximately $\mathcal{O}(PqN_{max}M_{max})$. Since the DDSP-based estimator does not consider the angular sparsity nature of the system like the 3D-SOMP-based estimator, it makes the computational complexity of the DDSP-based estimator lower than that of the 3D-SOMP-based estimator at approximately $\mathcal{O}(qN_{max}M_{max}\log P)$.

According to Table 4.1 and Table 4.2, the proposed DDSP-based estimator shows a lower computational complexity cost than the 3D-SOMP because the proposed DDSP-based estimator's nonzero entries of the sparse signal decay slowly [76], and the proposed DDSP-based estimator, does not consider sparsity in the angle domain, which results in low pilot overhead as no extra pilots are required to get the angle domain supports. Moreover, there is an achievement of further reduction in the computational complexity cost of the proposed DDSP-based estimator by the fast convergence rate of the estimator. As a result, it lowers the number of iterations to reach good performance.

Table 4.1: Pilot overhead values for a scenario in OTFS massive MIMO

Channel Estimator	**Pilot overhead**	**Numerical Values** **(q=80, G_M= M_{max}=600, G_N= N_{max}=12, P=6, D=q/10)**
Traditional impulse-based estimator	$qN_{max}M_{max}$	≈576 000*symbols*
3D-SOMP-based estimator	$N_{max}PD\log G_N G_M q$	≈3 318*symbols*
Proposed DDSP-based estimator	$N_{max}P\log G_N G_M q$	≈415*symbols*

Table 4.2: Computational complexity values for a scenario in OTFS massive MIMO

Channel Estimator	**Computational Complexity**	**Numerical Values** **(q=80, M_{max}=600, N_{max}=12, P=6)**
Traditional impulse-based estimator	$\mathcal{O}(M_{max}q^2)$	≈3 840 000
3D-SOMP-based estimator	$\mathcal{O}(PqN_{max}M_{max})$	≈3 456 000
Proposed DDSP-based estimator	$\mathcal{O}(qN_{max}M_{max}\log P)$	≈448 215

4.4 Simulation Results

This section presents the performance evaluation of the proposed DDSP channel estimation technique in a single transmitting urban macro-cell with one single antenna receiving user equipment to lower computational complexity. The system used in the simulation to evaluate the DDSP estimator has a carrier frequency of 2.15 GHz and is operating in FDD. In this work, there is an evaluation of the 15kHz sub-carrier spacing of the system, and the cyclic prefix rate used to alleviate inter-symbol interference is 16.6 micro-seconds [1],[18]. The simulations explore the OTFS modulation scheme, which operates efficiently and effectively in high-Doppler scenarios that can get to 500km/h or more [24]. As a result, the performance evaluations in this chapter include speeds from 10km/h to 660km/h, which are the envisaged speeds in wireless communications systems in both 5G and beyond 5G networks. According to [70], a traditional MIMO system has up to 8 antenna elements, and a massive MIMO system has at least 16 antenna elements. However, massive MIMO enables highly efficient and effective transmissions in systems with at least 64 antennas [71]. As a result, the performance evaluation in this section considers systems that range from 64-128 antenna elements to document the performance of the proposed estimator in a massive MIMO system.

For the performance index, mean square error, normalized by the signal power of the system referred to as NMSE, is employed. For the performance index, mean square error, normalized by the signal power of the system referred to as NMSE, is employed and expressed as follows:

$$NMSE = \frac{\|\hat{\boldsymbol{H}} - \boldsymbol{H}\|^2}{\|\boldsymbol{H}\|^2}, \tag{4.6}$$

where the estimated channel is $\hat{\boldsymbol{H}}$ and $\boldsymbol{H}$ is the true channel of the system. Due to high-Doppler scenarios in the OTFS modulation scheme and a massive number of antennas in a massive MIMO system, addressing the pilot overhead ratio is still a big problem in this work. As a result, this section compares pilot overhead ratios of the traditional impulse response channel estimation scheme, the 3D-SOMP-based estimator [17], and the proposed DDSP scheme. Further, to establish which estimators reach the stable state faster, the convergence rate results of both the 3D-SOMP-estimator and proposed DDSP-based estimator are obtained. A quicker convergence rate is significant in higher-Doppler scenarios because the channel estimator that

reaches the stable state faster performs better in a system where the channel statistic changes rapidly [18].

Figure 4.1 shows the simulation results of the performance of the proposed DDSP-based estimator in comparison with both the traditional impulse-based estimator and the 3D-SOMP-based estimator in [17].

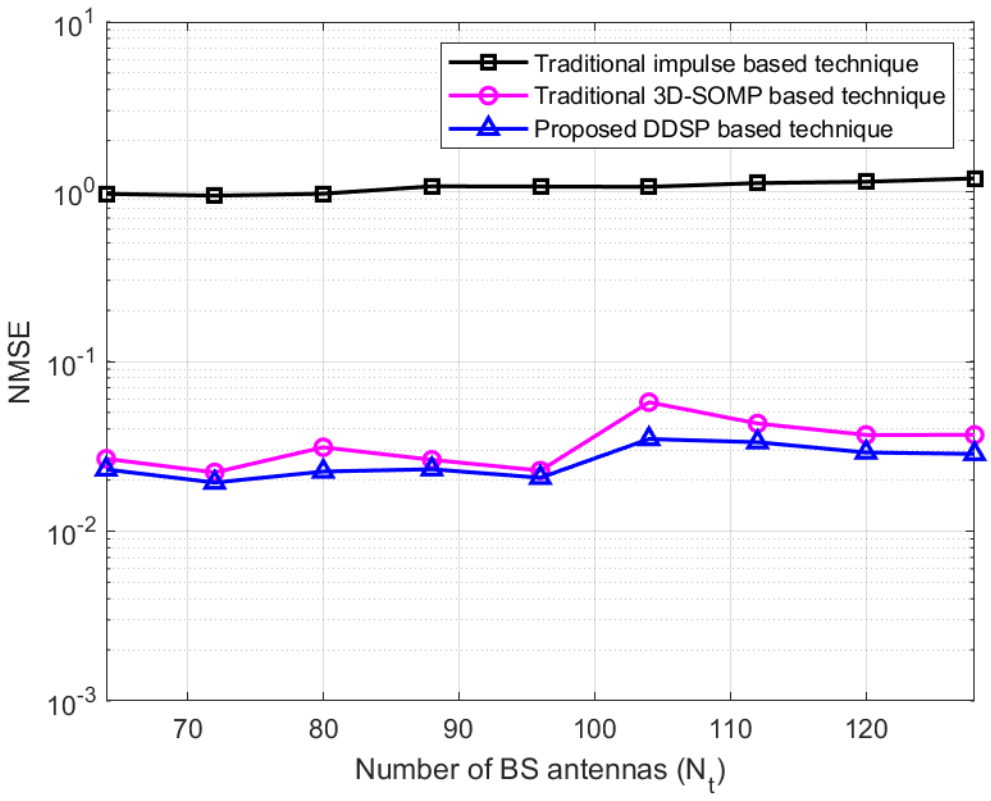

Figure 4.1: NMSE vs BS antennas for Traditional Impulse based channel estimation, 3D-SOMP channel estimation technique, and proposed Delay-Doppler Subspace Pursuit channel estimation technique

Different BS antennas (64-128 antennas) are employed to measure the NMSE performances of the various channel estimation schemes. The simulation of the results maintains a pilot overhead value of 0.5, SNR value of 5dB, and user equipment velocity of 360km/h. The NMSE performance of the traditional impulse-based channel estimation technique is consistently poor with the increase in the number of base station antenna elements. According to [17], this is mainly because the high number of antenna elements requires a higher pilot overhead ratio which is not the case for the system as the value of pilot overhead is maintained at 0.5. However, there is a difference in the performance between the traditional impulse-based channel estimation technique and the 3D-SOMP-based estimator [17] and the proposed DDSP-

based estimator. The proposed DDSP-based estimator shows a better performance gap (NMSE of about 0.0058 to 0.0246) than the 3D-SOMP-based estimator mainly because the DDSP-based estimator converges slightly faster to reach a stable state than the 3D-SOMP-based estimator and DDSP-based estimator estimates the channel from a limited quantity of random projections makes DDSP-based estimator use lesser pilots to estimate the channel as the base station antenna elements increase compared to the 3D-SOMP-based estimator.

Different pilot overhead ratios are varied, as shown in Figure 4.2, to see their impacts on NMSE performances of the algorithms in consideration.

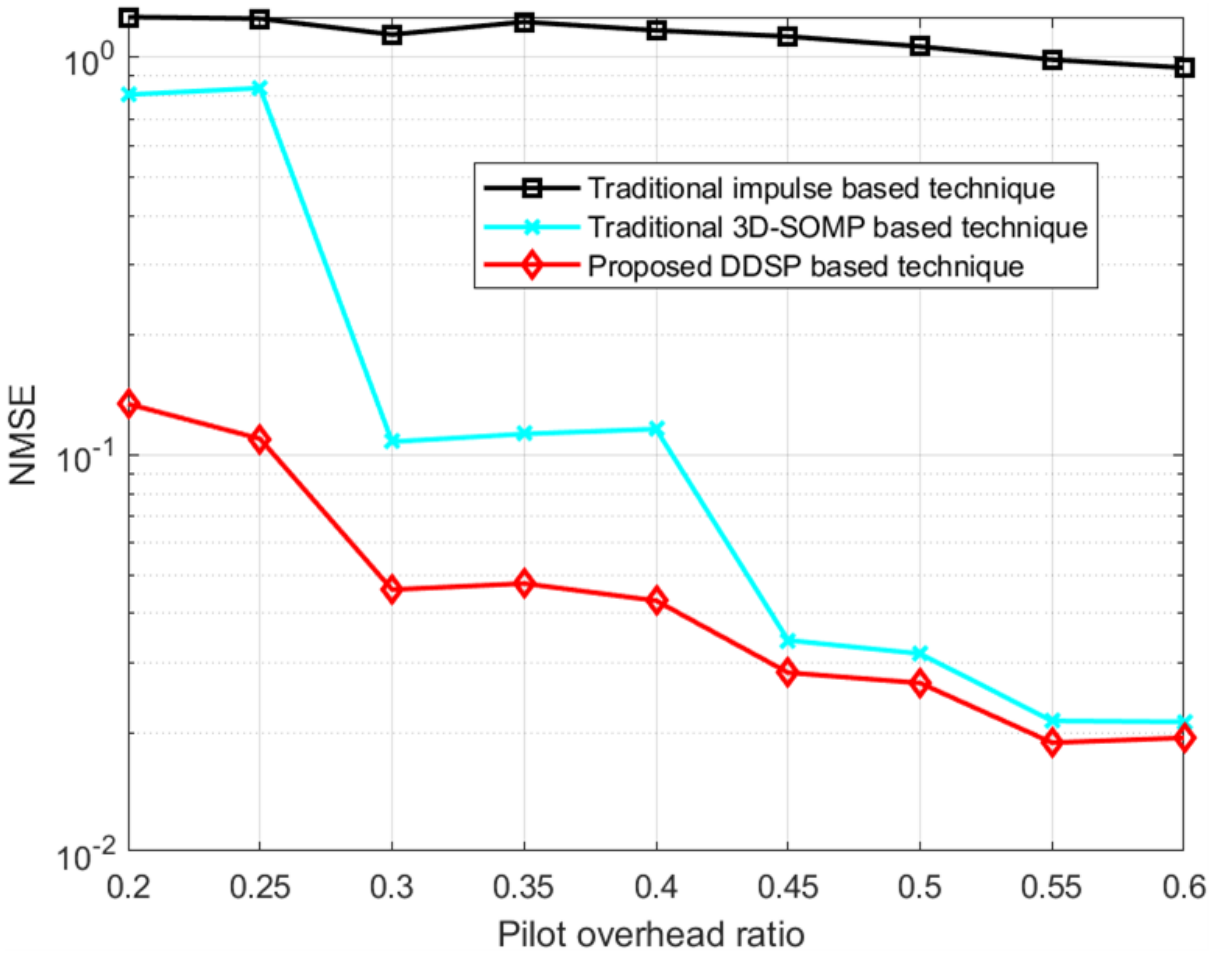

Figure 4.2: NMSE vs Pilot overhead ratio for Traditional Impulse based channel estimation, 3D-SOMP channel estimation technique, and proposed Delay-Doppler Subspace Pursuit channel estimation technique

The simulation of the results maintains 80 antenna elements at the base station. The simulation also maintains a 5dB SNR value and 360km/h user equipment velocity, which is close to the maximum speeds of some high-speed trains [1]. According to Figure 4.2, the 3D-SOMP-based estimator and the DDSP-based estimator improve NMSE performance with the increase in the

pilot overhead ratio. There is a significant difference of NMSE value of about 0.791 to 0.875 between the performance of the traditional impulse-based estimator and 3D-SOMP-based estimator and DDSP-based estimator mainly because of the higher Doppler the scenario, combined with many base station antennas presented by the system, makes it difficult for the traditional impulse-based channel estimation technique to keep track of the rapidly changing channel. It eventually causes higher inter-symbol interference and inter-carrier interference performance degradation. The 3D-SOMP-based estimator and the DDSP-based estimator display similar performance in higher pilot overhead ratios (45% going upwards). On the other hand, from 20% to 45% pilot overhead ratio, the DDSP-based estimator exhibits improved performance than the 3D-SOMP-based estimator, and this is due to the ability of the DDSP-based estimator to perform better in noisy regimes when employed for signal recovery [76] and this allows the DDSP-based estimator to be more efficient when operating under high Doppler scenarios and in a system with more antennas.

In Figure 4.3, the SNR ratio values are varied to show their effects on NMSE performance of the various channel estimators considered in high-Doppler scenarios (360km/h), 80 base station antennas, and constant pilot overhead ratio (50%). The DDSP-based estimator, 3D-SOMP-based estimator, and traditional impulse-based algorithms reach almost constant NMSE performances with the rise of SNR values. However, the 3D-SOMP-based estimator and DDSP-based estimator show better NMSE performance than the traditional impulse-based estimator, with the increase of SNR values in high-Doppler scenarios, due to high interference in the traditional impulse-based estimator [17]. Specifically, at NMSE of $10^{-1.7}$, the proposed DDSP estimator exhibits performance gains of about 5dB over the 3D-SOMP-based estimator. The proposed DDSP-based estimator's performance improves and gets better than the 3D-SOMP-based estimator as SNR values increase due to its ability to continuously update the correct subspace, which makes NMSE performance better in noisy regimes as it requires lesser pilot overhead and reduces interference in the high number of antennas in high-Doppler scenarios [76],[77].

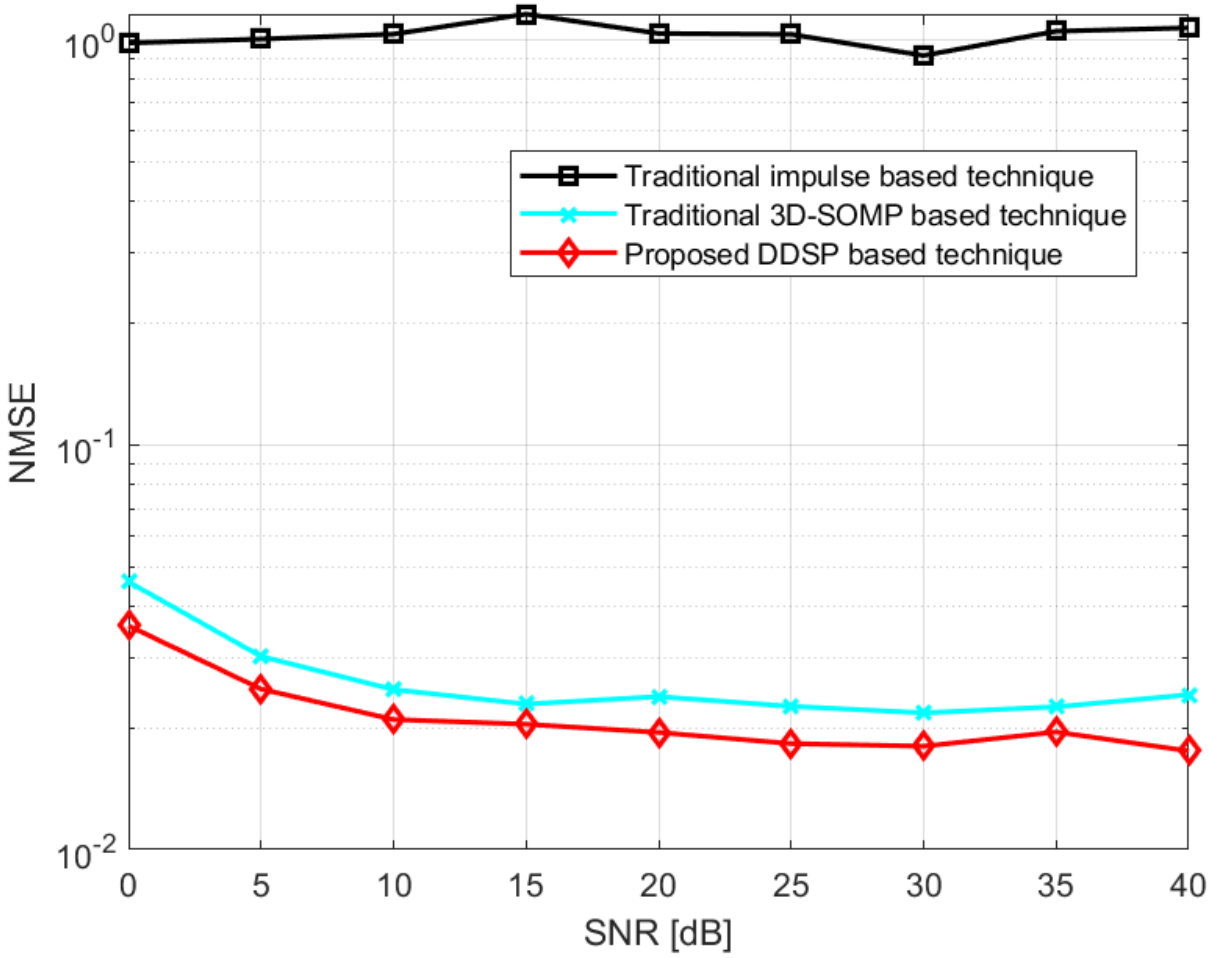

Figure 4.3: NMSE vs SNR ratio for Traditional Impulse based channel estimation, 3D-SOMP channel estimation technique, and proposed Delay-Doppler Subspace Pursuit channel estimation technique

According to Figure 4.4, the traditional impulse-based technique shows abysmal NMSE performance in high-Doppler scenarios in a system with a high number of antennas because the high Doppler spread causes inter-carrier interference in the system, which makes the system require a higher pilot overhead ratio which is not the case in the system considered in this chapter as the pilot overhead ratio is kept constant at 50% and SNR at 5dB. As a result of the high pilot overhead required, the traditional impulse-based technique will have low throughput, which is not favorable in 5G and beyond 5G wireless communication networks. The 3D-SOMP-based estimator and the proposed DDSP-based estimator have significantly better NMSE performance than the traditional impulse-based estimator. Results from the 3D-SOMP-based estimator and the proposed DDSP-based estimator's ability to keep up with the fast-varying channel properties introduced by high-Doppler scenarios are presented in this chapter. The proposed DDSP-based estimator displays better performance than the 3D-SOMP-based

estimator because it operates in noisy regimes, which gives it better and more accurate signal reconstruction [76],[77]. However, as the velocities of the users increase, the NMSE values of the 3D-SOMP-based estimator and the proposed DDSP-based estimator appear to be converging, and this can be improved by increasing the SNR value or pilot overhead ratio in the proposed DDSP-based estimator.

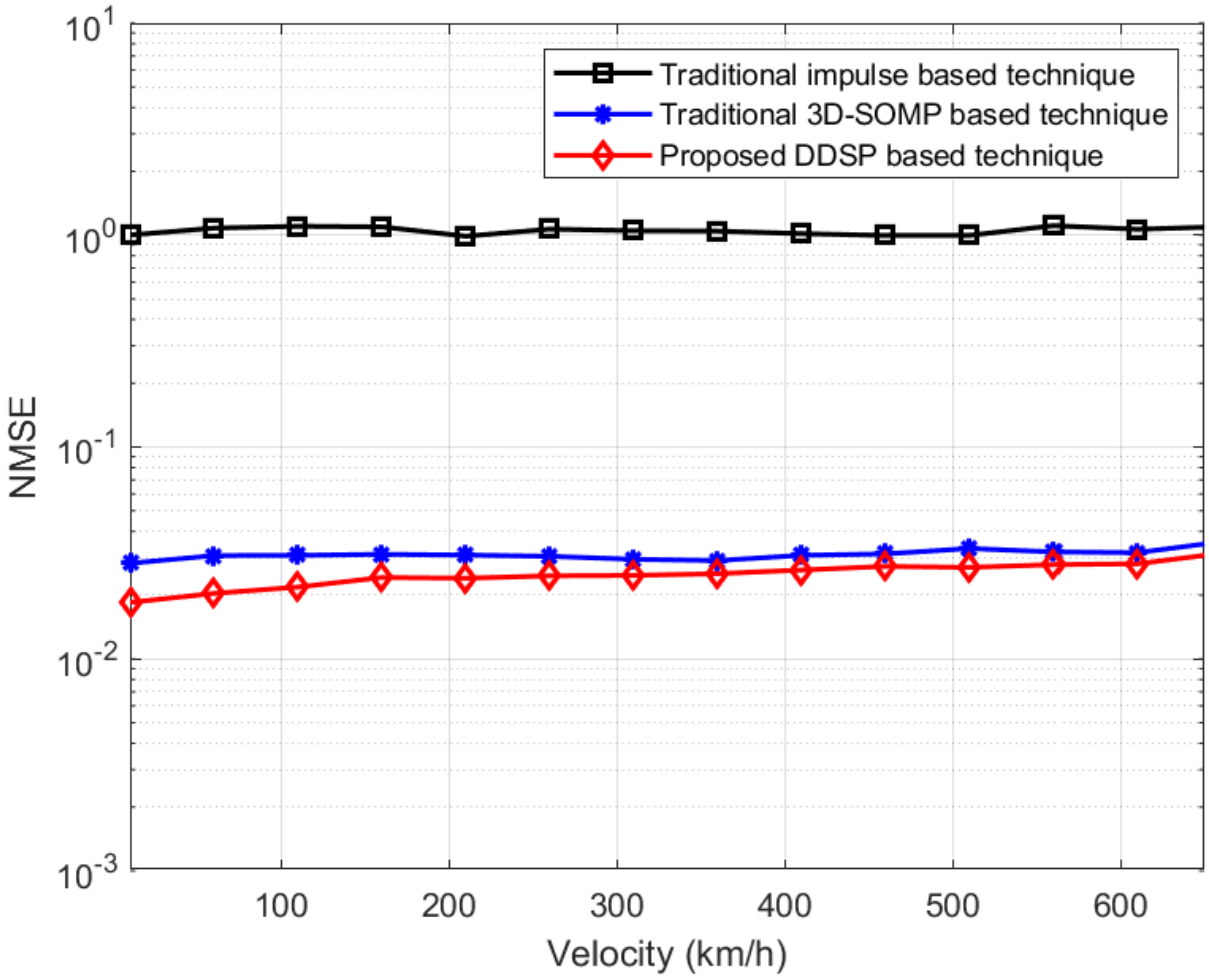

Figure 4.4: NMSE vs velocity for Traditional Impulse based channel estimation, 3D-SOMP channel estimation technique, and proposed Delay-Doppler Subspace Pursuit channel estimation technique

Figure 4.1 to Figure 4.4 shows close NMSE performance of the 3D-SOMP-based channel estimator and the DDSP-based channel estimator with variation of velocity, SNR values, pilot overhead and number of BS antennas. Figure 4.5 shows NMSE against number of iterations to show which of the two channel estimators converges to a minimum NMSE performance quicker. For the results shown in Figure 4.5, the antenna elements are kept at 80 elements, SNR

value is maintained at 5dB, pilot overhead is maintained at 50%, and velocity is maintained at 360km/h. The 3D-SOMP-based estimator takes longer to converge to a more stable state than the proposed DDSP-based estimator. It takes the 3D-SOMP-based estimator about six iterations to reach its best NMSE value. On the other hand, the proposed DDSP-based estimator takes about two iterations to converge to a constant and stable NMSE performance. The difference in the convergence rate of the 3D-SOMP-based estimator and the proposed DDSP-based estimator is due to the high quantity of antenna elements, which causes high interference amongst antennas in the 3D-SOMP-based estimator due to lower overhead eventually degrades the NMSE performance.

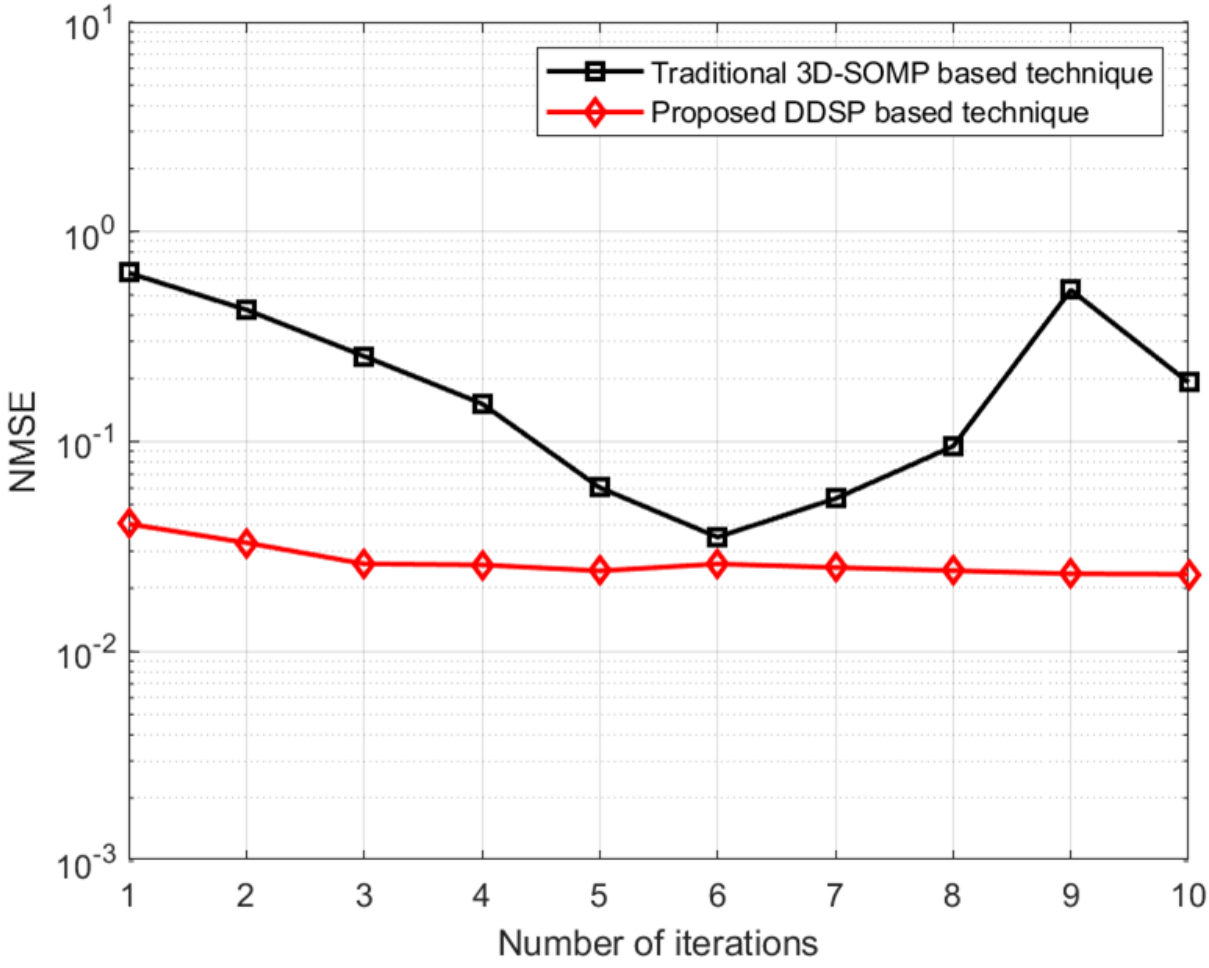

Figure 4.5: NMSE vs Number of iterations for 3D-SOMP channel estimation technique and proposed Delay-Doppler Subspace Pursuit channel estimation technique

Moreover, the proposed DDSP-based estimator displays better performance due to its regular refined spanned space, disregarding unreliable candidates in channel estimation. The difference

in NMSE from the beginning to the point of convergence for the 3D-SOMP-based estimator is about 0.5339. The difference in NMSE from the beginning to the point of convergence for the proposed DDSP-based estimator is about 0.0102, making the DDSP-based estimator a better channel estimation technique of choice for it does not take many iterations to reach a good error performance in high-Doppler scenarios. Table 4.1 and Table 4.2 illustrate the comparative complexity of the proposed DDSP-based estimator in both the pilot overhead and computational complexity cost. However, in Fig. 4.5, the proposed DDSP-based estimator shows convergence at two iterations. As a result, the complexities shown in Table 4.1 and Table 4.2 can be further reduced for the proposed DDSP-based estimator when the iteration value is reduced from 6 to 2 iterations.

4.5 Chapter Summary

This chapter proposed a new channel estimation scheme for OTFS Massive MIMO systems. The estimator is named the DDSP-based channel estimator. It is based on the traditional Subspace Pursuit-based estimator, and the time-variant OTFS massive MIMO channels are transformed into delay-Doppler OTFS massive MIMO channels. Due to the delay-Doppler sparsity nature of the channel in the OTFS massive MIMO system, the downlink channel estimation problem as a sparse signal recovery problem is formulated and is solved using the DDSP-based estimator. Simulations are performed based on the system model proposed in this chapter. The simulation results show that the DDSP-based estimator performs efficiently in the OTFS massive MIMO system within the scenarios considered as compared to traditional 3D-SOMP-based channel estimator and traditional impulse-based channel estimator. The proposed DDSP based estimator also incurred low pilot overheads. Lastly, the proposed DDSP estimator exhibits negligible computational complexity to the closely performing the 3D-SOMP proposed in the literature for OTFS Massive MIMO systems. Hence, the proposed DDSP-based estimator is a good candidate for OTFS massive MIMO-based 5G and beyond 5G wireless communications in both performance and computational complexity.

Chapter 5 – Proposed Gauss-Seidel-based MMSE Data Detection

5.1 Introduction

This chapter proposes a data detection scheme for the OTFS massive MIMO system. The goal is to present a method that approaches optimal performance and, at a low complexity cost, which makes it easier for hardware implementation. This chapter considers an uplink OTFS massive MIMO system model to accommodate a multi-user system model. The data detection technique aims to lower the computational complexity since the computational complexity is directly proportional to the number of UEs accommodated in the system. This chapter draws its proposed scheme from the traditional MMSE data detection technique. MMSE data detection is attractive for massive MIMO because it approaches optimal performances at a decent level of computational complexity cost. However, with MMSE data detection having matrix inversion, the proposed data detection aims at lowering the computational complexity of matrix inversion. Finally, the proposed data detection technique is evaluated through computer simulations, and the obtainable results are presented and discussed. The simulation results show that the proposed detection scheme approaches the performance of MMSE data detection and at lower computational complexity, which allows for it be used in less powerful/low-cost hardware and an excellent technique to consider in OTFS massive MIMO systems.

5.2 MMSE Data Detection for OTFS Massive MIMO

The OTFS massive MIMO system needs a reliable and efficient data detection technique to enjoy the benefits of channel estimation. A suitable data detection method will allow the receiver to detect the transmitted symbols with good error performance. One of the ultimate research problems available in exploring OTFS-based massive MIMO is to develop a more straightforward detection system that makes hardware implementation of OTFS massive MIMO system feasible and operate efficiently. Data detection of OTFS massive MIMO in high-Doppler scenarios is a daunting task because the channel parameters increase, computational complexity increases, and inter-user interference becomes severe with the increase in the number of UEs. There is an exhibition of outstanding error performance exhibited by non-linear detection methods like *maximum a posteriori*, sphere coding, K-best coding, and maximum likelihood. However, these non-linear detection techniques exhibit high computational complexity cost as the quantity of decision variables increases with the number of transmitted streams [28, 29]. Emerging technologies in 5G systems and beyond require

detectors to have low computational cost and low computational latency. As a result, that would make detectors with modest complexity acceptable because of stringent power and computational area constraints [28]. Thus, the necessity for near-optimal error performance and low complexity OTFS detectors to narrow the gap between algorithms and hardware implementation. Low complexity MMSE detection was used in the OTFS system to balance the trade-off between complexity and optimal performance [17].

Considering the OTFS system in Figure 1.3 with U single transmitter UEs and Q antennas at the base station receiver and in the system $\boldsymbol{y}$ is the received signal in the delay-Doppler domain, and $\boldsymbol{x}$ is the transmitted signal in the delay-Doppler domain as in equation (2.39). The receiver's task is to evaluate the log-likelihood ratio (LLR) values for the collected symbols $\boldsymbol{H}$ and $\boldsymbol{y}$ with a soft-output data detection algorithm. Typical MMSE detection can be computed as:

$$\hat{\boldsymbol{x}} = \boldsymbol{W}^{-1}\boldsymbol{y}^{MF}, \tag{5.1}$$

where $\boldsymbol{y}^{MF} = \boldsymbol{H}^{H}\boldsymbol{y}$ is the matched filter output, and the regularized *Gram matrix* $\boldsymbol{W}$ is $\boldsymbol{G} + \emptyset\boldsymbol{I}_u$ and *Gram matrix* $\boldsymbol{G} = \boldsymbol{H}^{H}\boldsymbol{H}$. The soft-input information LLRs can be computed from the estimated results for the soft-input channel after the estimation of the transmitted signal vector as:

$$\hat{\boldsymbol{x}} = \boldsymbol{F}\boldsymbol{x} + \boldsymbol{W}^{-1}\boldsymbol{H}^{H}\emptyset, \tag{5.2}$$

where $\boldsymbol{F} = \boldsymbol{W}^{-1}\boldsymbol{G}$ is the equivalent channel matrix and $\emptyset$ is the noise power. The estimated symbols can be written as $\hat{\boldsymbol{x}} = \boldsymbol{U}\boldsymbol{x} + \boldsymbol{t}$, where $\boldsymbol{U}$ is the effective channel gain and $\boldsymbol{t}$ is the noise plus interference (NPI).

5.3 Proposed Gauss-Seidel-based MMSE Data Detection for OTFS Massive MIMO

According to equation (5.2), MMSE data detection involves matrix inversion in uplink OTFS massive MIMO systems. Thus, making MMSE data detection undesirable when the number of decision parameters increases because of the increase in the decision process's computational complexity [30]. To alleviate the matrix inversion problem in uplink OTFS massive MIMO systems introduced by MMSE and reduce the complexity of data detection, a less complex

Neumann Series Expansion (NSE) soft detection MMSE method finds the necessary matrix inverse at a low complexity cost [31]. As much as NSE reduces the complexity of MMSE detection, there is an achievement of a marginal reduction in complexity in implementing NSE. To further lower the complexity of MMSE detection, this chapter proposes the Gauss-Seidel (GS)-based data detection technique in uplink OTFS massive MIMO, which has performance closer to that of the typical MMSE data detection method.

GS data detection aims at iteratively realizing the MMSE data detection without matrix inversion $\boldsymbol{W}^{-1}$. Diagonal-approximate initial solution introduced in the GS-based data detection method helps speed up the convergence rate and reduce the complexity of MMSE algorithm, as shown in the work presented in both [28] and [78]. The channel statistic $\boldsymbol{H}$ in (2.39) is a column full-rank and column asymptotically orthogonal, which makes *Gram matrix* $\boldsymbol{W}$ a Hermitian positive definite, as shown in [28] and [78]. As a result, $\boldsymbol{W}$ can be decomposed as:

$$\boldsymbol{W} = \boldsymbol{D} + \boldsymbol{L} + \boldsymbol{L}^{H}, \tag{5.3}$$

where $\boldsymbol{D}$, $\boldsymbol{L}$, and $\boldsymbol{L}^{H}$ represent diagonal component, the strictly lower triangular component, and the strictly upper triangular component $\boldsymbol{W}$, respectively. The GS method estimates the transmitted signal as follows:

$$\boldsymbol{x}^{(i)} = (\boldsymbol{D} + \boldsymbol{L})^{-1}(\overline{\boldsymbol{y}} - \boldsymbol{L}^{H}\boldsymbol{x}^{(i-1)}), \tag{5.4}$$

where i is the number of iterations, $\boldsymbol{x}^{(0)}$ is the initial solution, and $\overline{\boldsymbol{y}} = \boldsymbol{H}^{H}\boldsymbol{y}$.

The initial solution is very crucial for the convergence rate of the GS detection method, and it influences the complexity and the accuracy of the method when the number of iterations is small and finite. According to [28] and [78], $\boldsymbol{W}^{-1}$ is diagonally dominant. The bigger the transmitted signal, the more the domination of the diagonal elements of $\boldsymbol{W}^{-1}$ becomes more obvious, and the difference between $\boldsymbol{W}^{-1}$ and $\boldsymbol{D}^{-1}$ decreases. As a result, the initial solution in (5.4) can be approximately selected as:

$$\boldsymbol{x}^{(0)} = \boldsymbol{D}^{-1}\overline{\boldsymbol{y}}. \tag{5.5}$$

According to equation (5.5), there is an anticipation that the proposed diagonal approximate solution will be closer to the final MMSE evaluation compared with the traditional zero-vector initial solution. Thus, realizing the quicker convergence rate. The complexity of the MMSE and GS detection methods depends on the number of iterations required to find optimal performance values. There is an expectation of a quicker convergence rate in GS detection with the realization of equation (5.5). The faster the convergence rate, the fewer iterations are required to achieve optimal performance. As a result, there can be a reduction in the overall complexity of the GS detection. The proposed GS-based MMSE data detection method is summarised in Algorithm 5.1 as follows:

Algorithm 5.1: Proposed GS-based data detection

---

1. ***Input:*** Observation vector $\boldsymbol{y}$
   Delay-Doppler channel matrix $\boldsymbol{H}$
   Noise variance $\boldsymbol{N_0}$
   Iteration $\boldsymbol{K}$
2. ***Preprocessing***
   $\boldsymbol{W = H^H H + N_0 I_{MN}}$
   $\boldsymbol{W = D + Q}$ **and** $\boldsymbol{Q = L + L^H}$
3. ***Initialization***
   $\boldsymbol{x^0 = D^{-1} y^{MF}}$
4. ***(GS iteration)***
5. **for** i =1, 2, …, MN **do**
6. $\boldsymbol{x^{(i)} = (D + L)^{-1}(y^{MF} - L^H x^{(i-1)})}$
7. ***End*** **for**
8. ***Output:*** $\boldsymbol{x^{(i)}}$

5.4 Computational Complexity for the Data Detectors

The computational complexity of the GS-based data detection method and the NSE-based data detection method is based on the number of iterations (i) and the number of transmitting UEs. According to both [78] and [79], the computational complexity of NSE-based data detection is better than the one for MMSE data detection when the number of iterations $i \leq 3$. On the other hand, the computational complexity of NSE-based data detection reaches $\mathcal{O}((i-2)u^3)$ when

$i \geq 4$, which is even higher than the computational complexity of MMSE as shown in [78]. As a result, NSE-based data detection is not attractive in
uplink OTFS massive MIMO. By contrast, GS-based data detection can reduce complexity from $\mathcal{O}(u^3)$ to $\mathcal{O}((i+2)u^2 + 4u)$ as stipulated in both [28] and [78]. This makes GS-data detection more attractive as it lowers complexity cost and can exhibit close operational performance with the increase in the number of UEs compared to MMSE data detection. NSE-based data detection approaches the optimal performance of MMSE data detection when $i > 4$, which makes NSE unattractive when implementing uplink OTFS massive MIMO because the increase in the number of iterations also increases the complexity cost.

Table 5.1: Computational complexity values for a scenario in OTFS massive MIMO

Data Detector	**Computational Complexity**	**Numerical Values (u=16, i=4)**
NSE-based data detection	$\mathcal{O}((i-2)u^3)$	≈8 192
MMSE data detection	$\mathcal{O}(u^3)$	≈4 096
Proposed GS-based MMSE data detection	$\mathcal{O}((i+2)u^2 + 4u)$	≈1 600

5.5 Simulation Results

This section presents the performance evaluation of the proposed GS-based detection technique in the OTFS massive MIMO system. According to [70], a traditional MIMO system has up to 8 antenna elements, and a massive MIMO system has at least 16 antenna elements. However, massive MIMO enables highly efficient and effective transmissions in systems with at least 64 antenna elements, as detailed in [71]. As a result, the performance evaluation in this section considers systems with base station antennas up to 256 to document the performance of the proposed GS-based detection method in the OTFS massive MIMO system. For the performance index, there is the rate at which errors occur in the transmission of the OTFS symbols, BER, in the OTFS massive MIMO system. The simulation assumes the availability

of perfect CSI at the BS for the uplink OTFS massive MIMO system with UEs traveling at an average speed of 360km/h to focus on the computational complexity and error performances of the techniques considered in this chapter. The goal is to improve BER performance by increasing in receiving base station antennas. As a result, this section compares the BER of the traditional MMSE detection method NSE-based data detection and the proposed GS-based data detection method with the increase in SNR values, number of base station antennas, or the number of iterations. This is crucial because the proposed GS-based data detection method can achieve almost similar error performance to MMSE. However, at a lower computational complexity, it will be easier to implement the uplink OTFS massive MIMO system in high-Doppler scenarios where the channel statistic changes rapidly, as suggested in [18].

Figure 5.1 presents the simulation results of the proposed GS-based data detection method's performance compared to NSE-based data detection and the MMSE-based data detection method.

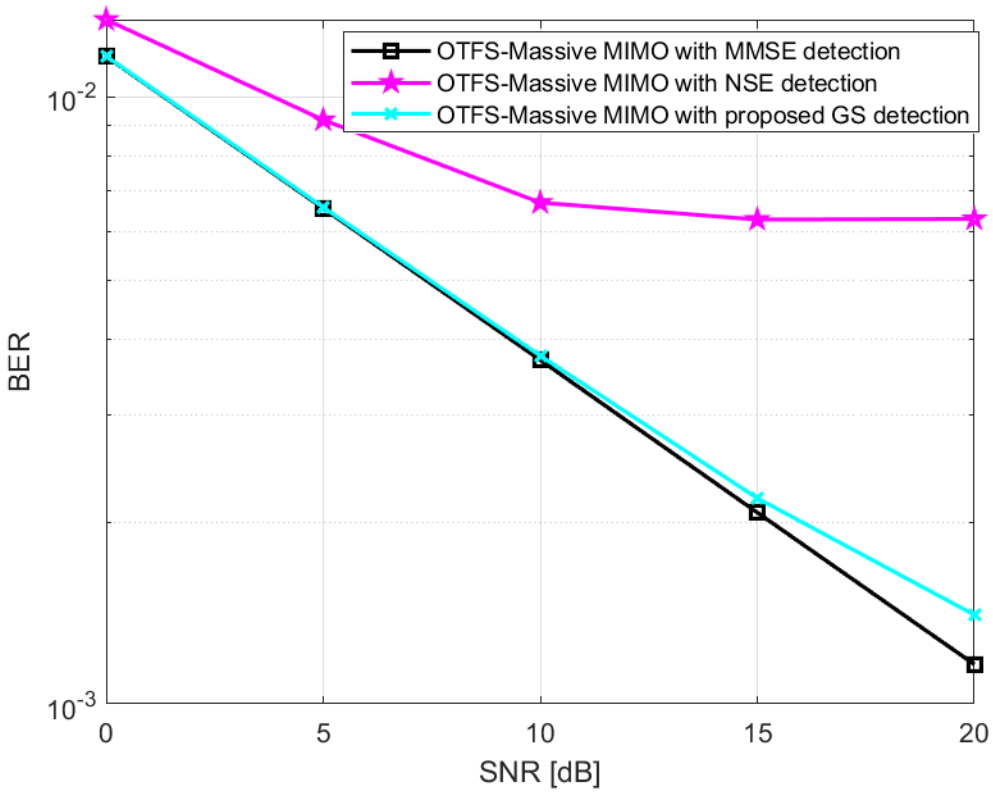

Figure 5.1: BER vs SNR for Traditional MMSE data detection, NSE-based data detection and proposed GS-based data detection

Different values of SNR (between 0dB to 20dB) are used to measure the BER of the data detection methods and to show their effectiveness in data transmission in OTFS massive MIMO, which is a required attractive trait in 5G systems and beyond. However, the number of UEs was kept constant at 16, and the number of base station antenna elements was kept at 256. The proposed GS-based data detection method displays a BER performance than NSE-based data detection. The proposed GS-based data detection shows performance closer to MMSE data detection. Figure 5.1 shows that NSE-based data detection is not attractive, especially when the SNR values increase. On the other hand, GS-based data detection exhibits relatively close performance to MMSE-based data detection, which makes GS-based data detection more attractive in uplink OTFS massive MIMO.

Figure 5.2 shows the different performances of the proposed GS-based data detection technique, NSE-based data detection, and MMSE-based technique under different iterations.

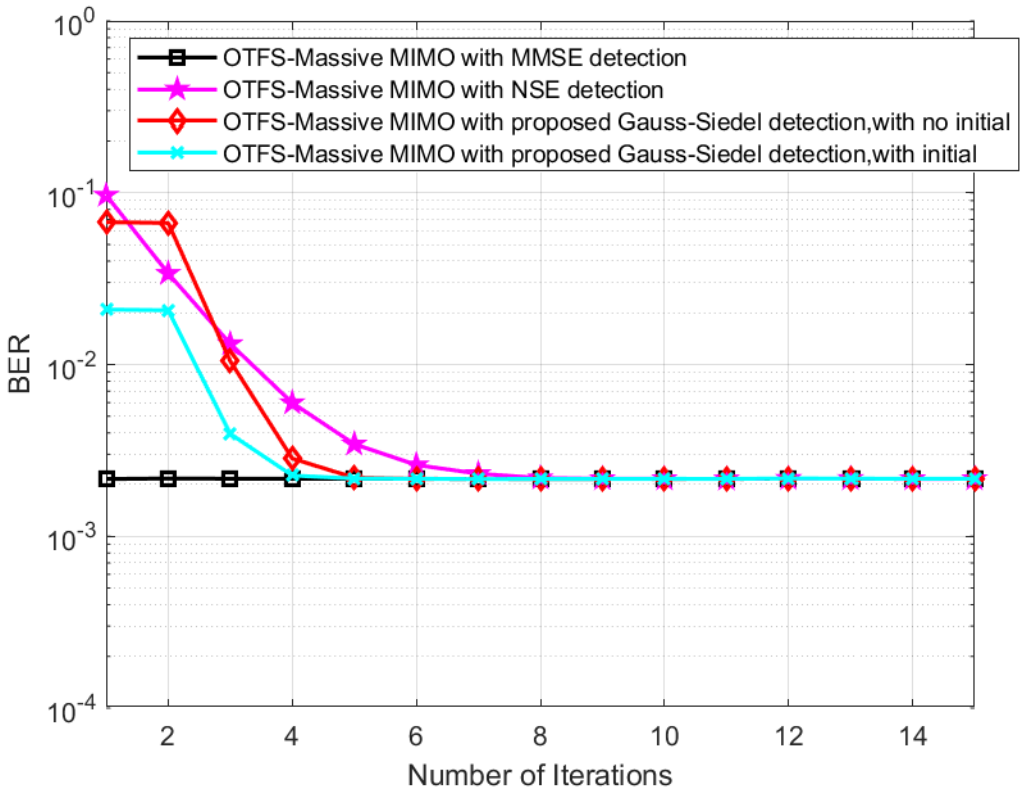

Figure 5.2: BER vs Number of iterations for Traditional MMSE data detection, NSE-based data detection, and proposed GS-based data detection

The proposed GS-based data detection with initial demonstrates a faster convergence rate as compared to the proposed GS-based data detection with zero initial and NSE-based data

detection. The three detection methods maintain an almost similar performance at a higher number of iterations (greater than 8). It takes NSE-based data detection about eight iterations to converge to the MMSE data detection performance, and according to [28] and [78], when the number of iterations of NSE-based data detection is greater than 4, computational complexity is relatively closer to the computational complexity of MMSE data detection. As a result, NSE-based data detection is less attractive at higher iterations because it does not demonstrate any merits compared to MMSE data detection. The proposed GS-based data detection technique takes about five iterations with the initial GS solution and about six iterations for one with no initial GS solution. This makes GS-based data detection more attractive because faster convergence is attractive. After all, the system reaches optimal performance with fewer iterations.

Figure 5.3 shows the BER performances of proposed GS-based data detection in comparison with the traditional linear MMSE-based data detection under different values of SNR (from 0dB to 20dB), two different iteration values (3 and 4), and different initial values for GS solutions.

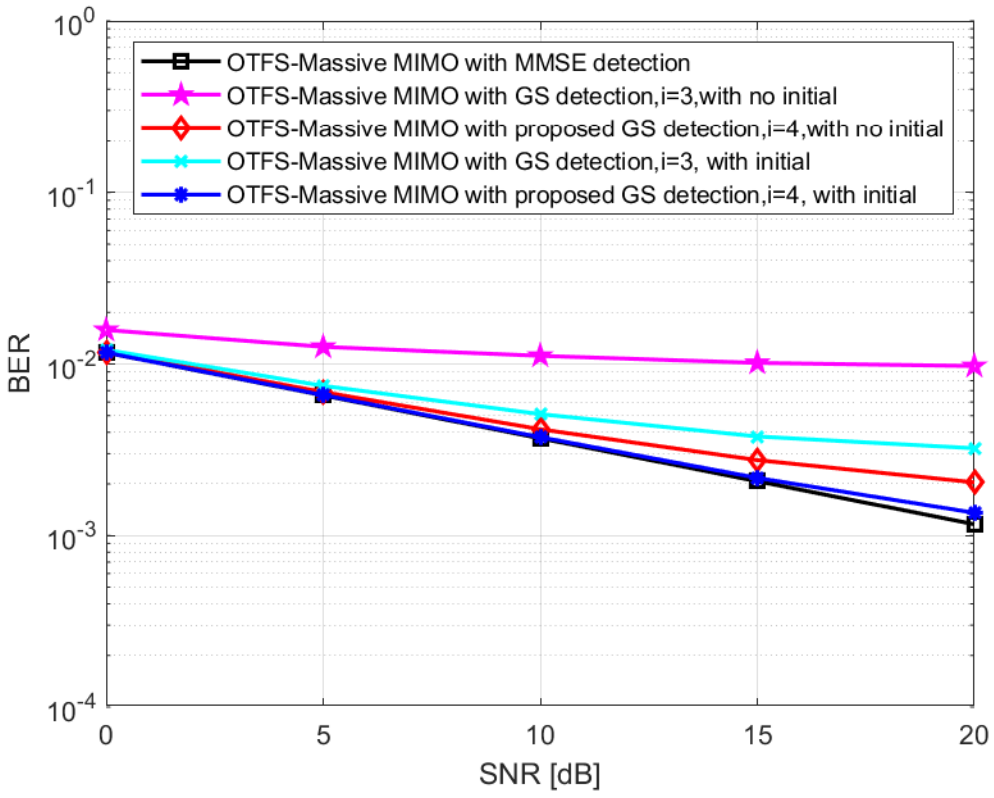

Figure 5.3: BER vs SNR for Traditional MMSE data detection and proposed GS-based data detection without initial GS solution and with initial GS solution

For the results in this figure, 256 antennas at the base station and 16 transmitting UEs are considered. The proposed GS-based data detection method with an initial GS solution demonstrates better BER performance than the one with no initial GS solution. The results in Figure 5.3 further support those of Figure 5.2, as they show that GS-based data detection with an initial GS solution has better performance than the GS-based data detection with no initial GS solution. GS-based data detection with an initial solution exploits the fact that the MMSE filtering matrix is diagonally dominant for massive MIMO systems, as detailed in [28]. That makes the technique's performance much closer to MMSE data detection's performance.

In Figure 5.4, the number of base station antennas is varied from 16 antennas to 256 antennas to measure the BER performances of the various data detection methods considered in this chapter.

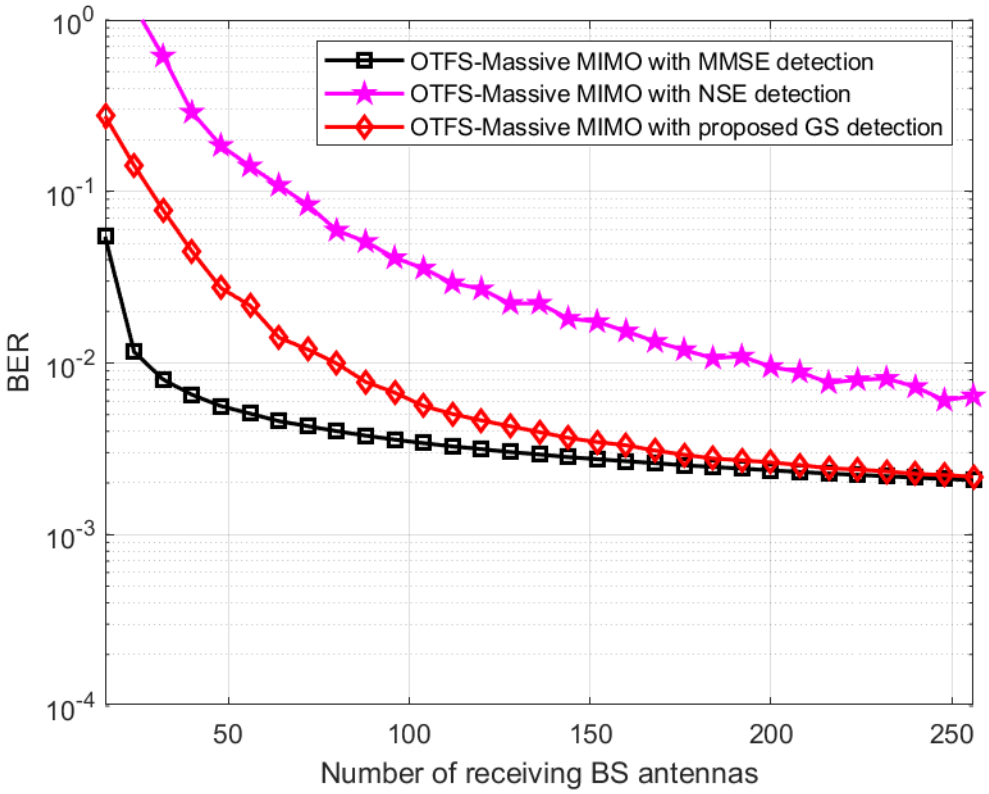

Figure 5.4: BER vs Number of receiving base station antennas for Traditional MMSE data detection, NSE-based data detection and proposed GS-based data detection

For these results, both the number of UEs and the value of SNR are fixed at 16 and 15dB, respectively. From the simulation results, it is evident that the increase in the number of antennas increases the level of performance of all the methods in consideration. NSE-based data detection method exhibits the poorest performance compared to the other two detection techniques. As the quantity of base station antennas increases to over 100, the performance of the proposed GS-based data detection technique converges to the performance for MMSE data detection. Thus, increasing the number of base station antennas for the GS-based data detection technique is more attractive in OTFS massive MIMO systems.

The proposed GS-based detection is expected to have lower implementation complexity than the NSE-based detection and the traditional linear MMSE detection method. Figure 5.5 shows that with the increase in the number of UEs, the proposed GS-based data detection has the lowest computational complexity. As a result, this makes the proposed GS-based data detection technique to be more appealing as low complexity cost allows for it to be used in less powerful/low-cost hardware implementation for uplink OTFS massive MIMO, which makes it more economical and feasible to implement in the real world.

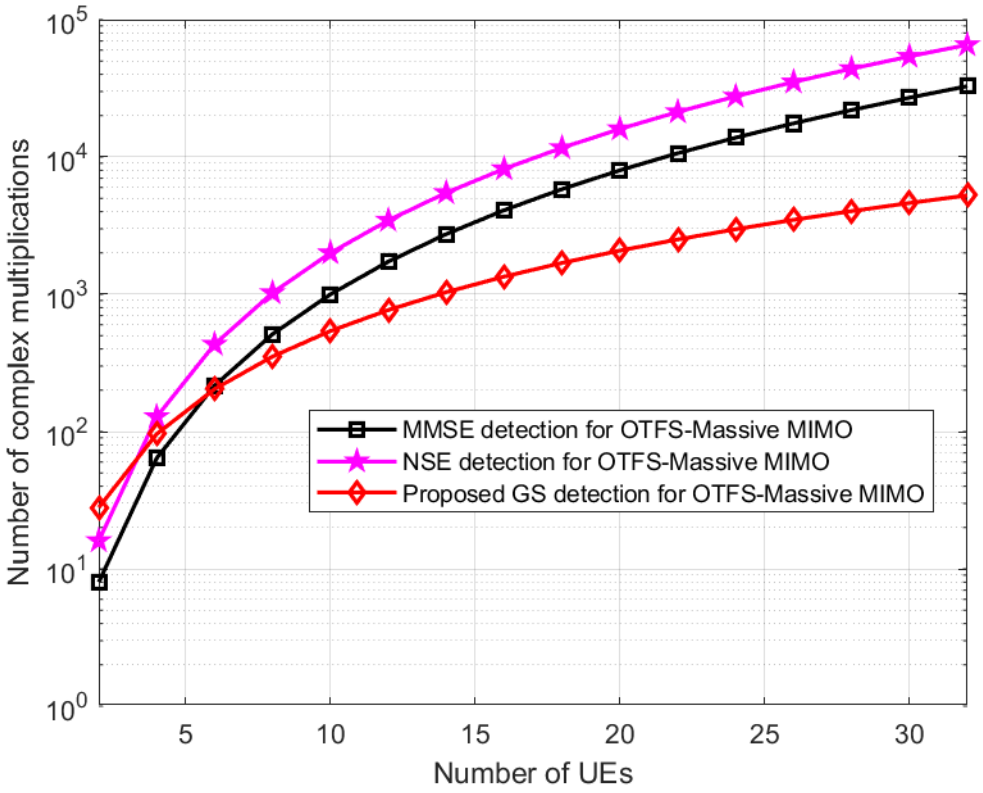

Figure 5.5: Number of complex multiplications vs number of UEs for Traditional MMSE data detection, NSE-based data detection, and proposed GS-based data detection

5.6 Chapter Summary

This chapter presents the implementation of the proposed GS-based data detection method for the transmitted symbols in the uplink OTFS massive MIMO systems. Due to the complexity of the OTFS massive MIMO system, an uplink linear data detection problem with associated low computational complexity cost is formulated in this chapter. The formulated problem was solved using the GS-based data detection technique. Since the MMSE-based data detection method shows optimal and less complex implementation, the proposed GS-based data detection was aimed at reducing the implementation complexity of the MMSE data detection, which eventually makes the OTFS massive MIMO feasible in 5G systems and beyond 5G. Simulation results show that the proposed GS-based data detection method performs efficiently in the OTFS massive MIMO system for the various OTFS massive MIMO system within the scenarios considered. The proposed GS-based data detection exhibits much lower computational complexity than the closely performing MMSE-based data detection earlier presented in the literature for OTFS massive MIMO systems. Hence, the proposed GS-based data detection technique is a good compromise for data detection for OTFS massive MIMO-based 5G and beyond 5G wireless communications in terms of performance and computational complexity.

Chapter 6 - Conclusions and Future Work

This chapter summarizes and concludes the works presented in this dissertation by outlining the contributions of the results obtained and paving the way for future research in this research area. As outlined in Chapter 1 in the research question, this research aimed to improve the efficiency of the OTFS massive MIMO by implementing a compressive sensing-based channel estimation technique. As a result, the study's goal in this research was to design a channel estimation technique with low computational complexity cost, low pilot overhead ratio, and good error performance. However, to fully enjoy the benefits of good channel estimation and better the efficiency of the OTFS massive MIMO system, the research further focused on developing a low complex linear data detection method which allows for it to be used in less powerful/low-cost hardware implementation and optimal performance.

Chapter 1 of the dissertation outlined the background of the research problem by providing more detailed information on the technologies in question (OTFS, massive MIMO, OTFS massive MIMO, and data detection in massive MIMO). By exploring the past and present works in the technologies, it was easier to identify the gaps in the literature. As a result, there was the identification and articulation of the research problem. Finally, there was the documentation of the structure of the remaining part of the dissertation.

Chapter 2 provided an overview of the technologies in question. The chapter also documented the literature review on channel estimation, data detection, massive MIMO, OTFS massive MIMO and formulated system models. As a result, this led to the formulation of the system models for channel estimation and data detection of the OTFS massive MIMO system.

Chapter 3 presents the CoSaMP-based channel estimator with interleaving to exploit the collective sparsity nature of the delay-Doppler channel in OTFS massive MIMO and improve the efficiency of transmission and receiving of information in OTFS massive MIMO systems. Finally, the results were outlined and discussed.

Chapter 4 presents the DDSP-based channel estimator to improve the efficiency of transmission and receiving of information in OTFS massive MIMO systems. The DDSP-based channel estimator was introduced to exploit the sparsity nature of the OTFS massive MIMO system, and the results were outlined and discussed.

Chapter 5 presents the GS-based MMSE data detection method to improve hardware implementation of OTFS massive MIMO and at the same time guarantee almost optimal performance, and the results were outlined and discussed.

According to the simulation results and discussions in Chapter 3, it is evident that the proposed CoSaMP-based channel estimator with interleaving is efficient compared to the 3D-SOMP-based compressive sensing channel estimator in terms of error performance. The proposed CoSaMP-based channel estimator proves efficiency by requiring fewer pilot symbols to reach optimal performance. In conclusion, the results provide evidence that the proposed channel estimation scheme improves the efficiency of compressive sensing algorithms in OTFS massive MIMO systems.

According to the simulation results and discussions in Chapter 4, the proposed DDSP-based channel estimator is efficient compared to some of the compressive sensing-based channel estimators compared to OTFS massive MIMO systems. DDSP-based channel estimator has a faster convergence rate, reaching its optimal performance with fewer iterations. Moreover, it also proves to be efficient by requiring fewer pilot symbols to achieve optimal performance. Additionally, the proposed DDSP-based channel estimator reaches optimal error performance with low complexity cost, which allows for it to be used in less powerful/low-cost hardware implementation easier. The corresponding results prove that the proposed channel estimation scheme improves the efficiency of compressive sensing algorithms in OTFS massive MIMO systems.

The simulation results and discussions in Chapter 5 provide evidence of the proposed data detector being efficient in OTFS massive MIMO. A good data detector can harvest the benefits of good channel estimation with fewer errors and low complexity cost. MMSE data detector does provide optimal performance but at a higher computational complexity cost. As a result, a GS-based data detector was proposed, and the results are a testament to its efficiency with optimal performance at lesser iterations. Additionally, there is an achievement of lower computational complexity cost, which improves the hardware implementation and eventually can be more economical than MMSE data detector in OTFS massive MIMO systems.

As much as the proposed CoSaMP-based CE and DDSP-based CE techniques are less complex and demonstrates quicker optimization, it is still less precise as compared to blind CE techniques. Moreover, as much as interleaving enhances the proposed CoSaMP-based CE technique by improving the error performance of the OTFS massive MIMO systems, it still imposes a delay in the communication systems and increases noise in the systems.

The proposed GS-based MMSE data detection reduces the computational complexity of data detection in OTFS massive MIMO systems because it makes the process of detection of the transmitted symbols easier in a lesser number of iterations. On the other hand, GS-based data

detection guarantees convergence to traditional MMSE-based data detection for diagonally dominant, positive definite or symmetric matrix, which is sometimes not true.

In conclusion, it can be said, based on the various simulation results documented in this dissertation, that the proposed channel estimation schemes (the CoSaMP-based channel estimator and the DDSP-based channel estimator) could be recommended for the OTFS massive MIMO wireless communication systems due to their good performances and the corresponding lower computational complexity cost when compared with their counterparts considered in this dissertation. Further, the proposed GS-based data detector could be considered a good compromise in terms of both performance and computational complexity cost for implementation in the uplink OTFS massive MIMO wireless communication systems.

6.1 Future Research Work

Though this dissertation has presented channel estimation techniques based on compressive sensing principles and signal detection employing linear detection algorithm, some possible areas remain for future consideration in the OTFS Massive MIMO systems. These are as listed below.

- Designing a delay-Doppler precoder at the transmitter to improve the efficiency of OTFS massive MIMO systems. By designing an efficient precoder, the system can enhance the capacity of the system by being able to accommodate more users with less inter-user interference.
- Approaching the transmitter precoder for OTFS massive MIMO as an optimization problem to improve the precoding process before the channel statistic changes.
- Combining optimized precoder for OTFS massive MIMO with linear detector to decrease propagation in unwanted areas and improve hardware implementation.
- Combining optimized precoder for OTFS massive MIMO with joint channel estimation and data detection to improve the transceiver design of the system.

References

[1] Zhang M, Wang F, Yuan X, and Chen L, "2D Structured Turbo Compressed Sensing for Channel Estimation in OTFS Systems," in *IEEE International Conference on Communication Systems (ICCS)*; Chengdu, China,2018.

[2] Raviteja P, Phan KT, Hong Y, and Viterbo E, "Interference Cancellation and Iterative Detection for Orthogonal Time Frequency Space Modulation," *IEEE Transactions on Wireless Communications* , vol. 17, no. 10, pp. 6501-6515, 2018.

[3] Surabhi GD, Augustine RM, and Chockalingam A, "On the Diversity of Uncoded OTFS Modulation in Doubly-Dispersive Channels," *IEEE Transactions on Wireless Communications*, vol. 18, no. 6, pp. 3049-3063, 2019.

[4] RezazadehReyhani A, Farhang A, Ji M, Chen RR, and Farhang-Boroujeny, "Analysis of Discrete-Time MIMO OFDM-Based Orthogonal Time Frequency Space Modulation," *IEEE International Conference on Communications (ICC)*: Kansas City, MO, USA, 2018.

[5] Raviteja P, Phan KT, Hong Y, and Viterbo E, "Embedded Delay-Doppler Channel Estimation for Orthogonal Time Frequency Space Modulation," *IEEE 88th Vehicular Technology Conference (VTC-Fall)*: Chicago, IL, USA, 2018.

[6] Neelam SG and Sahu PR, "Error performance of OTFS in the presence of IQI and PA Nonlinearity," *IEEE National Conference on Communications (NCC)*: Kharagpur, India, 2020 .

[7] Surabhi GD and Chockalingam A, "Low-Complexity Linear Equalization for OTFS Modulation," *IEEE Communications Letters*, vol. 24, no. 2, pp. 330-334, 2020.

[8] Khammammetti V and Mohammed SK, "OTFS-Based Multiple-Access in High Doppler and Delay Spread Wireless Channels," *IEEE Wireless Communications Letters*, vol. 8, no. 2, pp. 528-531, 2019.

[9] Surabhi GD, Ramachachandran MK and Chockalingam A, "OTFS Modulation with Phase Noise in mmWave Communications," *IEEE 89th Vehicular Technology Conference (VTC2019-Spring)*: Kuala Lumpur, Malaysia, 2019.

[10] Liu Y, Zhang S, Gao F, Ma J and Wang X, "Uplink-Aided High Mobility Downlink Channel Estimation Over Massive MIMO-OTFS System," *IEEE Journal On Selected Areas In Communications*, vol. 38, no. 9, pp. 1994-2009, 2020.

[11] Lajos Hanzo, Y Akhtman, Wang L, Ming J, "MIMO-OFDM for LTE, Wi-Fi and WiMax," *John Wiley and Sons, Ltd*, Publication, 2011; https:// 10.1002/9780470711750.

[12] X. Fernando and N Hassan, "Massive MIMO Wireless Networks: An Overview," www.mdpi.com/journal/electronics, 2017.

[13] Madalina-Georgiana B, Voicu C and Halunga S, "The performance of an uplink Massive MIMO OFDM-based multiuser system with LDPC coding when using relays," *IEEE 25th International Symposium for Design and Technology in Electronic Packaging (SIITME)*: Cluj-Napoca, Romania,2019.

[14] K. Deergha Rao and B.K Kartheek, "Comparative Performance Analysis of OMP and SABMP for Massive MIMO OFDM Channel Estimation," *5th IEEE Uttar Pradesh Section International Conference on Electrical, Electronics and Computer Engineering (UPCON)*: Gorakhpur, India,2018.

[15] Ming Jiang and Lajos Hanzo, "Multiuser MIMO-OFDM for Next-Generation Wireless Systems," *Proceedings of the IEEE,* vol. 95, no. 7, pp. 1430-1469, 2007.

[16] Zhao L, Zhao H, Zheng K, Xiang W, "Massive MIMO in 5G Networks: Selected Applications," *Springer Briefs in Electrical and Computer Engineering*, Publication, 2018.

[17] Shen W, Dai L, An J, Fan P and Heath RW Jr., "Channel Estimation for Orthogonal Time Frequency Space (OTFS) Massive MIMO," *IEEE Transactions On Signal Processing,* vol. 67, no. 16, pp. 4204-4217, 2019.

[18] Hadani R, Rakib S, Kons S, Tsatsanis M, Monk A, Ibars C, Delfeld J, Hebron Y, Goldsmith AJ, Molisch AF, and Calderbank K, "Orthogonal Time Frequency Space Modulation," *IEEE Wireless Communications and Networking Conference*: San Francisco, CA, USA, 2017.

[19] M. Kollengode Ramachandran and A. Chockalingam, "MIMO-OTFS in High-Doppler Fading Channels: Signal Detection and Channel Estimation," *IEEE Global Communications Conference (GLOBECOM)*: Abu Dhabi, United Arab Emirates, 2018.

[20] Shashank Tiwari, Suvra Sekhar Das, and Vivek Rangamgari, "Low complexity LMMSE Receiver for OTFS," *IEEE Communications Letters,* vol. 23, no. 12, pp. 2205 - 2209, 2019.

[21] Shashank Tiwari and Suvra Sekhar Das, "Circularly Pulse Shaped Orthogonal Time Frequency Space Modulation," *IEEE Electronic Letters*, vol. 56, no. 3, pp. 157 - 160, 2020.

[22] Changyoung A and Heung-Gyoon. R, "Design and Performance Evaluation of Spectral Efficient Orthogonal Time Frequency Space System," in *IEEE 2nd 5G World Forum (5GWF)*: Dresden, Germany, 2019.

[23] Noura Derria Lahbib, Maha Cherif, Moez Hizem, and Ridha Bouallegue, "Massive MIMO Uplink Channel Estimation using Compressive Sensing," *IEEE International Conference on Software, Telecommunications and Computer Networks (SoftCOM)*: Split, Croatia, 2019.

[24] Jwo-Yuh Wu, "How Much Coherent Interval Should be Dedicated to Non-Redundant Diagonal Precoding for Blind Channel Estimation in Single-Carrier Block Transmission?," *IEEE Transactions on Wireless Communications,* vol. 9, no. 8, pp. 2560 - 2574, 2010.

[25] Latif Ullah Khan, M. Haseeb Zafar, M. Irfan Khattak, and Naeem Khan. A novel channel estimation error minimizing interpolation technique for OFDM systems, *IEEE 9th International Symposium on Communication Systems, Networks & Digital Sign (CSNDSP)*: Manchester, UK, 2014.

[26] Divya Pandey and Neelam Dewangan. Performance Analysis of Pilot Assisted Channel Estimation in OFDM, *IEEE International Conference on Computer, Communication and Control (IC4)*: Indore, India, 2015.

[27] Raviteja P, Phan KT, and Hong Y, "Embedded Pilot-Added Channel Estimation for OTFS in Delay-Doppler Channels," *IEEE Transactions on Vehicular Technology* , vol. 68, no. 5, pp. 4906-4917, 2019.

[28] Chuan Zhang, Zhizhen Wu, Christoph Studer, Zaichen Zhang, and Xiaohu You, "Efficient Soft-Output Gauss-Seidel Data Detector for Massive MIMO Systems," *IEEE Transactions on Circuits and Systems I: Regular Papers* , vol. 68, no. 12, pp. 5049 - 5060, 2018.

[29] Albreem MA, Alsharif MH, and Kim S, "A Robust Hybrid Iterative Linear Detector for Massive MIMO Uplink Systems ," *Symmetry,* 2020, 12, 306; https://doi:10.3390/sym12020306.

[30] Yin B, Wu M, Studer C, Cavallaro JR, and Dick C. Implementation trade-offs for linear detection in large-scale MIMO systems, *IEEE International Conference on Acoustics, Speech, and Signal Processing*: Vancouver, BC, Canada, 2013.

[31] Yin B, Wu M, Wang G, Dick C, Cavallaro JR, and Studer C, "A 3.8 Gb/s LARGE-SCALE MIMO DETECTOR FOR 3GPP LTE-ADVANCED," *IEEE International Conference on Acoustics, Speech, and Signal Processing (ICASSP)*: Florence, Italy, 2014.

[32] Weiyu Xu, Youzheng Wang, Zucheng Zhou, and Jing Wang, "Joint ML Channel Estimation and Data Detection for STBC via Novel Sphere Decoding Algorithms," *IEEE 61st Vehicular Technology Conference*: 2005.

[33] J. L. L. Morales, S Roy, "On Joint Detection and Channel Estimation over Rank-Deficient MIMO Links with Sphere Decoding," *IEEE 12th Canadian Workshop on Information Theory*: 2011.

[34]. T. Thaj and E. Viterbo, "Low-Complexity Linear Diversity-Combining Detector for MIMO-OTFS," in IEEE Wireless Communications Letters, doi: 10.1109/LWC.2021.3125986.

[35]. T. Thaj and E. Viterbo, "Low Complexity Iterative Rake Decision Feedback Equalizer for Zero-Padded OTFS Systems," in IEEE Transactions on Vehicular Technology, vol. 69, no. 12, pp. 15606-15622, Dec. 2020, doi: 10.1109/TVT.2020.3044276.

[36] H. R. Palally, S. Chen, W. Yao, and L. Hanzo, "PARTICLE SWARM OPTIMISATION AIDED SEMI-BLIND JOINT MAXIMUM LIKELIHOOD CHANNEL ESTIMATION AND DATA DETECTION FOR MIMO SYSTEMS," *IEEE/SP 15th Workshop on Statistical Signal Processing*: 2009.

[37] M. Abuthinien, S. Chen, and L. Hanzo, "Semi-blind Joint Maximum Likelihood Channel Estimation and Data Detection for MIMO Systems," *IEEE Signal Processing Letters,* vol. 15, pp. 202 - 205, 2008.

[38] Constantinos Rizogiannis, Eleftherios Kofidis, Constantinos B. Papadias, Sergios Theodoridis, "SEMI-BLIND MAXIMUM LIKELIHOOD JOINT CHANNEL ESTIMATION / DATA DETECTION FOR MIMO FADING CHANNELS," *IEEE 7th Workshop on Signal Processing Advances in Wireless Communications*: 2006.

[39] O Oyerinde and S.H Mneney, "Review of Channel Estimation for Wireless Communication Systems," *IETE Technical Review,* vol. 29, no. 4, pp. 282-298, 2012.

[40] Tae-Yoon Park, Young-Shin Ahn, Ung Heo, Im-Bin Lim, and Jae-Ho Choi, "Pilot-assisted technique on LDPC-coded COFDM-CDMA in frequency-selective multipath fading channels ," *IEEE 9th Asia-Pacific Conference on Communications (IEEE Cat. No.03EX732)*: Penang, Malaysia, 2003.

[41] Zijun Zhao, Xiang Cheng, Miaowen Wen, Liuqing Yang, and Bingli Jiao, "Constructed Data Pilot-assisted Channel Estimators for Mobile Environments," *IEEE Transactions on Intelligent Transportation Systems,* vol. 16, no. 2, pp. 947 - 957, 2014.

[42] Gao F, Xing C, and Wang G, "Channel Estimation for Physical Layer Network Coding Systems," *Springer Briefs in Computer Science,* Publication, 2014.

[43] Hakan Dogan, Osman Sayl, and Erdal Panayirci, "Pilot Assisted Channel Estimation for Asymmetrically Clipped Optical OFDM over Visible Light Channels ," *IEEE International Black Sea Conference on Communications and Networking (BlackSeaCom)*: Varna, Bulgaria, 2016.

[44] Osamu Takyu, Takeo Yamasaki, and Yohtaro Umeda, "Scattered Pilot Assisted Channel Estimation for IFDMA," *IEEE 1st International Conference on Wireless Communication, Vehicular Technology, Information Theory and Aerospace & Electronic Systems Technology*: Aalborg, Denmark, 2009.

[45] Alexis Bazin, Bruno Jahan, and Maryline Hélard, "Impact of the Doppler Effect on the Capacity of Massive MIMO Uplink Systems: OFDM Versus FBMC/OQAM," *IEEE 24th International Conference on Telecommunications (ICT)*: Limassol, Cyprus, 2017.

[46] Jiang M, Huang S, Wen W, Liuqing Yang, and Bingli Jiao, "Adaptive Polar-Linear Interpolation Aided Channel Estimation for Wireless Communication Systems," *IEEE Transactions on Wireless Communications,* vol. 11, no. 3, pp. 920 - 926, 2012.

[47] Lorne Applebaum, Waheed U. Bajwa, A. Robert Calderbank, Jarvis Haupt, and Robert Nowak, "Deterministic Pilot Sequences for Sparse Channel Estimation in OFDM systems," *IEEE 17th International Conference on Digital Signal Processing (DSP)*: Corfu, Greece, 2011.

[48] Hu Feng, Li Jianping, and Cai Chaoshi, "A novel Semi-Blind Channel Estimation Algorithm for OFDM systems," *IEEE International Conference on Wireless Communications & Signal Processing*: 1-4, Nanjing, China, 2009.

[49] Wan F, Wei-Ping Z, and M.N.S Swamy, "A Closed-Form Semi-blind Solution to MIMO-OFDM Channel Estimation," *IEEE International Conference Neural Networks & Signal Processing*:Zhenjiang, China, 2008.

[50] Sangirov Gulomjon, Fu Y, Jamshid Sangirov, Fang Y, and Ahmad Olmasov, "A performamce analysis of optimized semi-blind channel estimation method in OFDM systems," *IEEE ICACT Transactions on Advanced Communications Technology (TACT)*, vol. 5, no. 5, pp. 907 - 912, 2016.

[51] Veria Havary-Nassab, Shahram Shahbazpanahi, Ali Grami, and Alex B. Gershman, "Experimental Performance Evaluation of Blind Channel Estimation for Orthogonal Space-Time Block codes," *5th IEEE Sensor Array and Multichannel Signal Processing Workshop*: Darmstadt, Germany, 2008.

[52] Karim Abed-Meraim and Yingbo Hua, "Blind identification of sparse multipath channels using cyclostationary statistics," *IEEE 9th European Signal Processing Conference (EUSIPCO 1998)*: Rhodes, Greece, 1998.

[53] Yun Ye and Saman S. Abeysekera, "Evaluating a Blind Channel Estimation Technique that uses a Hardware Efficient Equalizer," *IEEE International Symposium on Circuits and Systems (ISCAS)* : Kobe, 2005.

[54] Emmanuel Kanterakis and Wei Su, "Blind OFDM Parameter Estimation Techniques in Frequency-Selective Rayleigh Channels," *IEEE Radio and Wireless Symposium* : 2011.

[55] Simon G. Wood, Jr, Bernd-Peter Paris and Jill K. Nelson, "Channel Order Estimation via Sample Sorting," *IEEE 45th Annual Conference on Information Sciences and Systems* : Baltimore, MD, USA, 2011.

[56] Mohammad A. Khojastepour, Krishna Gomadam, and Xiaodong Wang, "Pilot-Assisted Channel Estimation for MIMO OFDM systems using theory of sparse signal recovery," *IEEE International Conference on Acoustics, Speech and Signal Processing* : Taipei, Taiwan, 2009.

[57] Shidong Zhou and Tingting Shi, "A novel pilot assisted channel estimation method for single-carrier systems," *14th IEEE Proceedings on Personal, Indoor and Mobile Radio Communications. PIMRC*: Beijing, China, 2003.

[58] Alireza Movahedian and Michael McGuire, "Efficient and Accurate Semiblind Estimation of MIMO-OFDM Doubly-Selective Channels," *IEEE 80th Vehicular Technology Conference (VTC2014-Fall)*: Vancouver, BC, Canada, 2014.

[59] Hu Feng, Jianping Fei, Yang Fei, and Zhang Shuai, "QR Decomposition-Based Semi-Blind MIMO Channel Estimation," *IEEE International Conference on Communications and Mobile Computing*: Shenzhen, China, 2010.

[60] Pappa M, Ramesh C, and Madhushri N. Kumar, "Performance Comparison of Massive MIMO and Conventional MIMO Using Channel Parameters," *IEEE International Conference on Wireless Communications, Signal Processing and Networking (WiSPNET)*: Chennai, India, 2017.

[61] Gao Z, Dai L, Dai W, and Wang Z. Kumar, "Block Compressive Channel Estimation and Feedback for FDD Massive MIMO," *IEEE Conference on Computer Communications Workshops (INFOCOM WKSHPS)*: 2015.

[62] F.A. Dietrich, M. Joham, and W. Utschick, "Joint Optimization of Pilot Assisted Channel Estimation and Equalization applied to Space-Time Decision Feedback Equalization," *IEEE International Conference on Communications*: 2005.

[63] Suvra Sekhar Das, Vivek Rangamgari, Shashank Tiwari, and Subhas Chandra Mondal, "Time Domain Channel Estimation and Equalization of CP-OTFS Under Multiple Fractional Dopplers and Residual Synchronization Errors," *IEEE Access* , vol. 9, pp. 10561 - 10576, 2020.

[64] P. Raviteja, Khoa T. Phan, and Yi Hong, "Embedded Pilot-Aided Channel Estimation for OTFS in Delay–Doppler Channels," *IEEE Transactions on Vehicular Technology* , vol. 68, no. 5, pp. 4906 - 4917, 2019.

[65] Yinghao Ge, Weile Zhang, Feifei Gao, Shun Zhang, and Xiaoli Ma, "High-Mobility Massive MIMO with Beamforming Network Optimization: Doppler Spread Analysis and Scaling Law," *IEEE Journal on Selected Areas in Communications*, vol. 38, no. 12, pp. 2889 - 2902, 2020.

[66] Nann Win Moe Thet, Tuncer Baykas, and Mehmet Kemal Ozdemir, "Performance Analysis of User Scheduling in Massive MIMO with Fast Moving Users," *IEEE 30th Annual International Symposium on Personal, Indoor and Mobile Radio Communications (PIMRC)*: 2019.

[67] Ali J. Al-Askery, Charalampos C. Tsimenidis, and Said Boussakta, "Fixed-Point Arithmetic Detectors for Massive MIMO-OFDM systems," *IEEE 23rd European Signal Processing Conference (EUSIPCO)*: 2015.

[68] Manish Mandloi and Vimal Bhatia, "Error Recovery Based Low-Complexity Detection for Uplink Massive MIMO Systems," *IEEE Wireless Communications Letters,* vol. 6, no. 3, pp. 302 - 305, 2017.

[69] Zhen Gao, Linglong Dai, Chenhao Qi, Chau Yuen, and Zhaocheng Wang, "Near-Optimal Signal Detector Based on Structured Compressive Sensing for Massive SM-MIMO," *IEEE Transactions On Vehicular Technology* , vol. 66, no. 2, pp. 1860 - 1865, 2017.

[70] Chataut R and. Akl R, "Massive MIMO Systems for 5G and beyond Networks—Overview, Recent Trends, Challenges, and Future Research Direction," *Sensors,* 2020, 20, 2753; https://doi:10.3390/s20102753, pp. 1-35.

[71] Byung-Jin L, Sang-Lim. J, Nam-il. K, and Kyung-Seok. K, "Enhanced Transmit-Antenna Selection Schemes for Multiuser Massive MIMO Systems," in *Wiley Hindawi, Wireless Communications and Mobile Computing*, 2017: https://doi.org/10.1155/2017/3463950.

[72] Hongyun Pan, Yanming Xue, Lidan Mei, and Fei Gao, "An improved CoSaMP sparse channel estimation algorithm in OFDM system," *IEEE International Conference on Signal Processing, Communications and Computing (ICSPCC)*, 2015.

[73] Yong Liao, Lei Zhao, Haowen Li, Fan Wang, Guodong Sun, "Channel Estimation Based on Improved Compressive Sampling Matching Tracking for Millimeter-wave Massive MIMO," *IEEE/CIC International Conference on Communications in China (ICCC)* , 2017.

[74] B. Lohini Priyanka, K. Rajeswari, S. J. Thiruvengadam, "MIMO-OFDM Channel Estimation using Distributed Compressed Sensing," *IEEE International Conference on Computational Intelligence and Computing Research* , 2014.

[75] David L. Donoho, “Compressed Sensing,” *IEEE Transactions On Information Theory*, vol. 52, no. 4, 2006.

[76] Wei Dai and Olgica Milenkovic, “Subspace Pursuit for Compressive Sensing Signal Reconstruction,” *IEEE Transactions on Information Theory* , vol. 55, no. 5, pp. 2230 - 2249, 2009.

[77] Kun Tan, Qun Wan, Anmin Huang, and Juan Wang, “A Fast Subspace Pursuit For Compressive Sensing,” *IET International Radar Conference*: , 2009.

[78] Dai L, Gao X, Su X, Han S, Chih-Lin I, and Wang Z, “Low-Complexity Soft-Output Signal Detection Based on Gauss–Seidel Method for Uplink Multiuser Large-Scale MIMO Systems,” *IEEE TRANSACTIONS ON VEHICULAR TECHNOLOGY*, vol. 64, no. 10, pp. 4839-4845, 2015.

[79] Wu M, Yin B, Vosoughi A, Studer C, Cavallaro JR, and Dick C, “Approximate Matrix Inversion for High-Throughput Data Detection in the Large-Scale MIMO Uplink,” *IEEE International Symposium on Circuits and Systems (ISCAS)*: 2013.